A Semi-Lagrangian approach for dilute non-collisional fluid-particle flows

Aude Bernard–Champmartin*[1], Jean-Philippe Braeunig †[2,3],
Christophe Fochesato‡[2,3], and Thierry Goudon§[1,4]

[1]Inria, Sophia Antipolis Méditerranée Research Centre, Project COFFEE
[2]CEA, DAM, DIF, F-91297 Arpajon, France
[3]LRC MESO, ENS Cachan,
61, avenue du Président Wilson, 94235 Cachan cedex, France
[4]Univ. Nice Sophia Antipolis, CNRS, Labo J.-A. Dieudonné, UMR 7351,
Parc Valrose, F-06108 Nice, France

January 15, 2014

Abstract

We develop numerical methods for the simulation of particulate flows where a dense phase and a dilute phase interact through drag forces. Semi-Lagrangian techniques are presented to handle the Vlasov-type equation which governs the evolution of the particles. We discuss several options to treat the coupling with the hydrodynamic system describing the dense phase, paying attention to strategies based on staggered discretizations of the fluid velocity.

1 Introduction

This paper is concerned with the numerical simulation of dilute suspensions. The modelling is motivated by many applications ranging from industrial processes to natural flows. For instance, the study of such flows is involved in the design of internal combustion engines and the improvement of their performances [47, 53, 67]. The problem is also relevant for the conception of fluidized beds [7] where particles are suspended in the fluid stream, in order

*achampmartin@gmail.com
†jean-philippe.braeunig@cea.fr
‡christophe.fochesato@cea.fr
§thierry.goudon@inria.fr

to promote contacts and exchanges (of mass or heat) between the particles and the fluid. Similar questions arise from nuclear energy security, and weapons physics purposes. Other applications cover the dynamics of biomedical sprays [3, 4, 30, 52], environmental studies on pollutant transport [28, 54, 55, 58, 65], the formation of sandstorms, sediment transport, the "white water" produced by breaking waves [48], dispersion of ash during volcanic eruptions [56], powder–snow avalanches [16], etc.

We adopt a statistical description of the dilute phase through the distribution function $f(t,x,v)$ of the particles in phase space. Here and below, x and v are independent variables that stand for the position and velocity variables, respectively, while t represents time. In this modelling, at any position both phases can be present, and, assuming that particles are spherically shaped with typical radius $r_{\rm d}$, $\frac{4}{3}\pi r_{\rm d}^3 \int f(t,x,v)\,{\rm d}v$ defines the local volume fraction occupied by the particles. The particle distribution function obeys the collisionless Vlasov equation (or Williams equation)

$$\partial_t f + \nabla_x \cdot (vf) + \nabla_v \cdot (\mathscr{F} f) = 0. \tag{1.1}$$

(Note that, since x and v are independent variables, $\nabla_x \cdot (vf) = v \cdot \nabla_x f$.) It is coupled to a hydrodynamic system describing the evolution of the dense phase through the drag force term $\mathscr{F}$. Denoting by $u(t,x)$ the velocity field of the dense phase, the drag force is proportional to the relative velocity

$$\mathscr{F} = D\ (u - v).$$

The coefficient D (homogenous to the inverse of a time) is given as a function of $|v-u|$, the expression of which might be quite complicated, depending on the physical characteristics of the flows [50, 53]. Our ideas extend to the general case, but for the sake of simplicity, we shall restrict the description of the scheme to the simple linear case where D is a positive constant (Stokes flows). In this case, its expression is $D = \frac{9\mu}{2r_{\rm d}^2\varrho_{\rm d}}$, where μ stands for the dynamic viscosity of the fluid, and $\varrho_{\rm d}$ the mass per unit volume of the droplets (see [19] and the references therein). In the momentum equation that prescribes the evolution of the velocity u, we find a source term that accounts for the drag force exerted by the particles on the fluid:

$$S(t,x) = m_{\rm d} \int D f(t,x,v)\ (v - u(t,x))\,{\rm d}v = m_{\rm d} \int v\ \nabla_v \cdot \Big(\mathscr{F} f(t,x,v)\Big)\,{\rm d}v,$$

where $m_{\rm d} = \frac{4}{3}\pi r_{\rm d}^3 \varrho_{\rm d}$ stands for the mass of the particles. (For Stokes flows note that $m_{\rm d} D = 6\pi\mu r_{\rm d}$.) The difficulty for the analysis and the numerical simulation can be ranked depending on the other modelling assumptions. In particular we can distinguish the following situations:

- We can consider the carrier fluid as compressible or incompressible, inviscid or viscous. It leads to a huge variety of PDEs systems, with quite distinct features. Here, we will restrict to compressible and inviscid flows, described by standard Euler equations, with a mere state law for defining the pressure. Furthermore, we will work with isentropic models; taking into account energy exchanges leads to further technicalities [12, 51]. The local well-posedness of this situation is investigated in [5]. For the analysis of coupling with the Navier-Stokes equation we refer the reader to [13].

- Interparticles collisions are neglected. On the same token, Brownian motion of the particles is in most of the applications negligible; however adding velocity-diffusion helps in dealing with asymptotic regimes, based on relaxation towards Maxwellian states [18, 38, 39, 41]. We also refer the reader to [42] for the derivation of such diffusion term based on the modelling of some "turbulence" effects. In this paper we shall only consider drag forces.

- According to the terminology introduced in [53], for very thin sprays, the back reaction of the particles can be neglected; for thin sprays the coupling is due to the momentum exchanges only. By constrast, dealing with thick sprays means that the volume occupied by the particles cannot be neglected in the mass and momentum balance for the fluid, which introduces further coupling terms. This work only deals with thin sprays, the extension to thick sprays will be discussed elsewhere [6].

It is worth pointing out that a simplified framework can be obtained by assuming that particles are mono-kinetic: $f(t,x,v) = n(t,x)\delta(v = \mathscr{V}(t,x))$. In turn, the macroscopic quantities $n, \mathscr{V}$ satisfy a pressureless system [15]. However, such a system is known to produce unphysical solutions, which do not capture the spreading of particles, nor the possible crossing of trajectories (simulation of crossing jets), see [44]. A pressure term can be introduced in the model, as a trace of particles interaction; for instance it models close packing effects intended to prevent the particle concentration to reach a certain threshold, see [8, 55, 54, 58] and the references therein.

The numerical simulation of the Vlasov equation in such fluid-particles systems is usually performed by Particle-In-Cell (PIC) methods [1, 54, 55, 58]. However, these techniques are known to be highly sensible to sampling errors. Recently, H. Liu, Z. Wang and R. O. Fox [49] developed a level-set approach. In plasmas physics, it turns out that grid methods can now be a serious alternative to PIC methods. In particular the Semi-Lagrangian framework has been developed with remarkable success [9, 14, 20, 26, 27, 33, 34, 35, 43, 59, 60]. Based on the similarity of their structure, we expect that Semi-Lagrangian methods can be applied to fluid-particles flows too. This paper is an attempt in this direction.

We shall use the interpretation of the Semi-Lagrangian method as a Finite Volume scheme: the numerical fluxes are defined through integration of the end-points of the cells over the characteristics and a suitable interpolation procedure. Of course, the main difficulty relies on the treatment of the coupling with the hydrodynamic system. We shall use a time–splitting method which can be interpreted as a prediction–correction algorithm. We have in mind the possible integration of the method in industrial codes, where hydrodynamics is treated with a Lagrange-projection method on staggered grids [1, 62], with a version of the so–called BBC scheme [23, 29, 45, 61, 68]. This leads to the difficulty of defining the discrete force term in (1.1) and in the momentum equation. Hence, the paper is organized as follows. We start by collecting a few properties of the equations. In particular, by contrast to systems arising in plasma physics, since the field $(x,v) \mapsto (v, D(u(t,x) - v))$ is not divergence free, the L^∞ estimate on the initial data is not conserved uniformly. Section 3 overviews the principles of the Semi-Lagrangian methods and we explain some technical choices that look relevant for our purposes. Section 4 details the time-splitting strategy, which is based on a prediction-correction approach. We also explain how to handle the space-discretization and several options are discussed for the source term. We begin with the simple case of a coupling with the Burgers equation, and our results can be compared to [49]. Then, we extend the scheme for a coupling with the isentropic Euler equations for thin sprays. Section 5 is devoted to numerical simulations.

2 Basic properties of the Vlasov equation and the coupling

From now on, we restrict ourselves to the one–dimension framework. (As far as we work with Cartesian grids, the extension to higher dimensions follows by reasoning direction-wise.)

Equation (1.1) needs to be completed by initial and boundary conditions. We thus set

$$f\Big|_{t=0} = f_0, \text{ a positive and integrable function.}$$

For the boundary conditions, throughout this paper we assume either periodicity or perfect reflection of the particles on the boundaries $x \in \{x_{\min}, x_{\max}\}$:

$$f(t, x_{\min}, v) = f(t, x_{\min}, -v) \text{ for } v > 0, \qquad f(t, x_{\max}, v) = f(t, x_{\max}, -v) \text{ for } v < 0.$$

It is convenient to associate to the particle distribution function f the following macroscopic quantities:

$$n(t,x) = \int f(t,x,v)\,\mathrm{d}v, \qquad \text{Density of the dilute phase,} \tag{2.2}$$

$$\mathscr{V}(t,x) = \frac{\int v f(t,x,v)\,\mathrm{d}v}{n(t,x)} = \frac{J(t,x)}{n(t,x)}, \qquad \text{Bulk particles velocity,} \tag{2.3}$$

$$K(t,x) = \frac{1}{2}\int v^2 f(t,x,v)\,\mathrm{d}v, \qquad \text{Kinetic energy of the particles.} \tag{2.4}$$

We can equally define the temperature by $n\theta(t,x) = \int (v - \mathscr{V}(t,x))^2 f(t,x,v)\,\mathrm{d}v \geq 0$. We remind that the particulate volume fraction is $\frac{4}{3}\pi r_{\mathrm{d}}^3 n(t,x)$.

Let us rewrite (1.1) in the following non conservative form

$$\partial_t f + v\partial_x(f) + D(|v-u|)(u-v)\partial_v(f) = \Gamma f, \tag{2.5}$$

with

$$\Gamma(t,x,v) = \partial_v\Big(D(|v-u(t,x)|)\ (v-u(t,x))\Big) = D(|v-u(t,x)|) + D'(|v-u(t,x)|)|v-u(t,x)|.$$

It is natural to assume that $z \mapsto D(z)$ is non decreasing and bounded from below by a positive constant; accordingly, Γ is bounded from below too. Neglecting any difficulty that could be related to the regularity of the fluid velocity, we introduce the characteristic curves defined by the ODE system

$$\begin{aligned} &\frac{\mathrm{d}}{\mathrm{d}s}X(s;t,x,v) = V(s;t,x,v), \quad &&\frac{\mathrm{d}}{\mathrm{d}s}V(s;t,x,v) = D(U(s;X(s;t,x,v)) - V(s;t,x,v)),\\ &X(t;t,x,v) = x, &&V(t;t,x,v) = v. \end{aligned}$$

Here $X(s;t,x,v)$ (resp. $V(s;t,x,v)$) represents the position (resp. the velocity) at time s of a particle which starts at time t from position x and velocity v. Then (2.5) can be recast as

$$\frac{\mathrm{d}}{\mathrm{d}s}\Big[\ln f(s, X(s;t,x,v), V(s;t,x,v))\Big] = \Gamma(s, X(s;t,x,v), V(s;t,x,v)).$$

Integrating between $s = t^1$ and $s = t = t^2$ yields

$$f(t^2,x,v) = f(t^1, X(t^1;t^2,x,v), V(t^1;t^2,x,v))\ \exp\Big(\int_{t^1}^{t^2}\Gamma(s, X(s;t,x,v), V(s;t,x,v))\,\mathrm{d}s\Big) \tag{2.6}$$

This formula will be at the basis of the Semi-Lagrangian scheme. In particlar, it implies that the total mass of the particles is conserved: we have

$$\iint f(t,x,v)\,\mathrm{d}v\,\mathrm{d}x = \iint f_0(x,v)\,\mathrm{d}v\,\mathrm{d}x.$$

In fact, the following local mass conservation law holds

$$\partial_t \int f\,\mathrm{d}v + \partial_x \int vf\,\mathrm{d}v = \partial_t n + \partial_x J = 0. \tag{2.7}$$

As a matter of fact, further useful estimates on the solution can be deduced from (2.6). For instance, in the specific case of Stokes flows ($\Gamma = D$ is constant), we deduce from this formula the following remarkable consequences:

- We have

$$\min_{x,v}(f(t^1,x,v))e^{D(t^2-t^1)} \le f(t_2,x,v) \le \max_{x,v}(f(t^1,x,v))e^{D(t^2-t^1)}. \tag{2.8}$$

  It expresses the trend of the particles velocity to concentrate to the bulk velocity, due to the drag forces [46].

- However, the L^p norms are not conserved when $p \neq 1$: $\|f(t)\|_{L^p} = e^{D(1-1/p)t}\|f_0\|_{L^p}$. In particular, the L^2 norm cannot be used to evaluate the numerical diffusion, as it is natural for the Vlasov equations of plasma physics [9, 34].

In the context of thin sprays, the Vlasov equation (1.1) will be coupled to the Euler system for the density $(t,x) \mapsto \rho(t,x)$ and the velocity $(t,x) \mapsto u(t,x)$ of the carrier fluid as follows. Let $\varrho_{\mathrm{f}} > 0$ be a typical mass per unit volume for the fluid. Mass and momentum balance lead to

$$\begin{aligned} &\partial_t\rho + \partial_x(\rho u) = 0,\\ &\varrho_{\mathrm{f}}\Big(\partial_t(\rho u) + \partial_x(\rho u^2)\Big) + \partial_x p = m_{\mathrm{d}} \int D(v-u)f\,\mathrm{d}v. \end{aligned} \tag{2.9}$$

Here and below, we shall restrict to the simple case of an isentropic gas law, where the pressure is given by

$$\rho \mapsto p(\rho) = k\rho^\gamma, \qquad k > 0,\ \gamma > 1.$$

For the boundary condition we assume $u(t,x_{\min}) = 0 = u(t,x_{\max})$. We observe that the total momentum is conserved since

$$\partial_t(\varrho_{\mathrm{f}}\rho u + m_{\mathrm{d}} n\mathscr{V}) + \partial_x(\varrho_{\mathrm{f}}\rho u^2 + m_{\mathrm{d}} n\mathscr{V}^2 + p + m_{\mathrm{d}} n\theta) = 0,$$

bearing in mind the relation $n\theta + n\mathscr{V}^2 = 2K$. We introduce the free–energy

$$\rho \mapsto \Phi(\rho) \text{ such that } \Phi''(\rho) = \frac{p'(\rho)}{\rho},$$

and we can check that the following total energy dissipation

$$\begin{aligned} \frac{\mathrm{d}}{\mathrm{d}t}\left\{\int\left(\frac{\varrho_{\mathrm{f}}}{2}\rho u^2 + \Phi(\rho)\right)\mathrm{d}x + m_{\mathrm{d}}\iint \frac{v^2}{2}f\,\mathrm{d}v\,\mathrm{d}x\right\}\\ = -\iint m_{\mathrm{d}} D|v-u|^2 f\,\mathrm{d}v\,\mathrm{d}x = -m_{\mathrm{d}} Dn(\theta + |\mathscr{V}-u|^2) \le 0 \end{aligned}$$

holds.

Similar manipulations can be performed in the simpler situation where the system (2.9) is replaced by the Burgers equation, as in [49]

$$\partial_t u + \partial_x(u^2/2) = \frac{m_{\rm d}}{\varrho_{\rm f}} \int D(v-u) f \,{\rm d}v. \tag{2.10}$$

The total momentum is conserved

$$\partial_t(\varrho_{\rm f} u + m_{\rm d} n \mathscr{V}) + \partial_x(\varrho_{\rm f} u^2/2 + m_{\rm d} n \mathscr{V}^2 + m_{\rm d} n\theta) = 0,$$

and the total kinetic energy is dissipated since

$$\partial_t(\varrho_{\rm f} u^2/2 + m_{\rm d} K) + \partial_x\Big(\varrho_{\rm f}\frac{u^3}{3} + m_{\rm d}\int \frac{v^3}{2} f \,{\rm d}v\Big) = -m_{\rm d} D n(\theta + |\mathscr{V}-u|^2) \le 0.$$

More generally, we can show that the system (1.1), (2.10) admits infinitely many entropies: for any convex function G, we show that

$$\frac{\rm d}{{\rm d}t}\Big\{\int \varrho_{\rm f} G(u)\,{\rm d}x + \iint m_{\rm d} G(v) f \,{\rm d}v\,{\rm d}x\Big\} = -\iint m_{\rm d} D(v-u)(G'(v)-G'(u)) f \,{\rm d}v\,{\rm d}x \le 0.$$

3 Semi–Lagrangian methods

We denote $L = x_{\max} - x_{\min}$ the length of the space domain. We introduce a space discretization made of N_x cells with constant step $\Delta x = \frac{L}{N_x} > 0$. Similarly, given a computational domain defined by minimal and maximal velocities $v_{\min}$ and $v_{\max}$ respectively, we consider N_v cells with constant step $\Delta v = \frac{v_{\max}-v_{\min}}{N_v} > 0$. (In practice we choose most of the time $v_{\min} = -v_{\max}$.) The cells are denoted $[x_{i-1/2}, x_{i+1/2}]$ and $[v_{j-1/2}, v_{j+1/2}]$ with centers $x_i = \frac12(x_{i+1/2} + x_{i-1/2})$ and $v_j = \frac12(v_{j+1/2} + v_{j-1/2})$, respectively. This defines a Cartesian grid of the (truncated) phase space. The discrete particle distribution function $f^k_{i,j}$ is stored at the center of the cells; it is intended to approximate the mean value

$$\frac{1}{\Delta v \Delta x}\int_{x_{i-1/2}}^{x_{i+1/2}}\int_{v_{j-1/2}}^{v_{j+1/2}} f(t^k, x, v)\,{\rm d}v\,{\rm d}x$$

at the discrete time t^k. We shall denote

$$\bar f^k(x,v) = \sum_{i,j} f^k_{i,j}\ \mathbf{1}_{[x_{i-1/2},x_{i+1/2})}(x)\ \mathbf{1}_{[v_{j-1/2},v_{j+1/2})}(v)$$

the stepwise functions associated to the discrete unknown. Accordingly, the discrete density and bulk velocity are also stored at the centers of the space-grid

$$n^k_i = \Delta v \sum_j f^k_{i,j}, \qquad J^k_i = n^k_i V^k_i = \Delta v \sum_j v_j f^k_{i,j}.$$

Due to its conservative form, equation (1.1) can be solved by using a directional splitting, considering separately

$$\partial_t f + \partial_x(vf) = 0, \tag{3.11}$$

and

$$\partial_t f + \partial_v(D(u-v)f) = 0. \tag{3.12}$$

Both equations belong to the general framework of transport equations:

$$\partial_t g + \partial_y(Ag) = 0, \tag{3.13}$$

with a given field $(t, y) \mapsto A(t, y)$.

3.1 Finite Volume framework, Forward and Backward methods

We assume that we have at hand the solutions of the ODE

$$\frac{\mathrm{d}}{\mathrm{d}s}Y(s;t,y) = A(s, Y(s;t,y)), \qquad Y(t;t,y) = y.$$

Then the solution of (3.13) satisfies

$$g(t,y) = g(s, Y(s;t,y))\ \mathscr{J}(s;t,y)$$

for any t, s, y with

$$\mathscr{J}(s;t,y) = \exp\left(\int_t^s (\partial_y A)(\sigma, Y(\sigma;t,y))\,\mathrm{d}\sigma\right)$$

the jacobian of the change of variable $z = Y(s;t,y)$, $\mathrm{d}z = \mathscr{J}(s;t,y)\,\mathrm{d}y$. Consequently, the conservation property can be written as follows

$$\int_a^b g(t,y)\,\mathrm{d}y = \int_{Y(s;t,a)}^{Y(s;t,b)} g(s,z)\,\mathrm{d}z. \tag{3.14}$$

These formulae are crucial to construct the Semi-Lagrangian scheme.

We work with Semi-Lagrangian methods that can be expressed as a Finite Volume scheme: given a grid with cells $[y_{m-1/2}, y_{m+1/2}]$, centered at y_m with constant size $\Delta y > 0$, we seek a relevant expression for updating

$$g_m^{k+1} = g_m^k - \frac{\Delta t}{\Delta y}(G_{m+1/2}^k - G_{m-1/2}^k), \tag{3.15}$$

the numerical unknown g_m^k being an approximation of the cell-average $\bar{g}_m^k = \frac{1}{\Delta y}\int_{y_{m-1/2}}^{y_{m+1/2}} g(t^k, y)\,\mathrm{d}y$. We distinguish

- The Backward Semi-Lagrangian method [35]

  We use the formula (3.14) with $t = t^{k+1}$, $s = t^k$, $a = y_{j-1/2}$, $b = y_{j+1/2}$ the endpoints of the cell: the left hand side is thus $\bar{g}_m^{k+1}$

  $$\bar{g}_m^{k+1} = \frac{1}{\Delta y}\int_{Y_{m-1/2}^{\mathrm{Back}}}^{Y_{m+1/2}^{\mathrm{Back}}} g^k(z)\,\mathrm{d}z,$$

  where we have set

  $$Y_{m+1/2}^{\mathrm{Back}} = Y(t^k; t^{k+1}, y_{m+1/2}).$$

Since $\bar{g}_m^k$ is the mean value of $g(t^k,\cdot)$ over the mth cell, we can write a formula which looks like (3.15)

$$\bar{g}_m^{k+1} = \bar{g}_m^k - \frac{\Delta t}{\Delta y}(\bar{G}_{m+1/2}^k - \bar{G}_{m-1/2}^k)$$

with the flux

$$\bar{G}_{m+1/2}^k = \frac{1}{\Delta t}\int_{Y_{m+1/2}^{\mathrm{Back}}}^{y_{m+1/2}} g(t^k,z)\,\mathrm{d}z = \frac{1}{\Delta t}\Big(\mathscr{G}^k(y_{m+1/2}) - \mathscr{G}^k(Y_{m+1/2}^{\mathrm{Back}})\Big),$$

$\mathscr{G}^k$ being a primitive of $g(t^k,\cdot)$. As a matter of fact we have

$$\mathscr{G}^k(y_{m+1/2}) = \Delta y \sum_{\mu=0}^{m} \bar{g}_\mu^k.$$

The numerical scheme (3.15) mimics these formulae: since the numerical unknown g_m^k is intended to approximate the cell average $\bar{g}_m^k$, we can still consider that in the numerical flux $\mathscr{G}^k(y_{m+1/2})$ is approached by $\Delta y\sum_{\mu=0}^m g_\mu^k$. What we need is a relevant definition of the approximation of the primitive $\mathscr{G}^k(Y_{m+1/2}^{\mathrm{Back}})$ at the foot of the characteristic coming backward from the interface $y_{m+1/2}$. It relies on an interpolation procedure.

- The Forward Semi-Lagrangian method

  We use the formula (3.14) with $t=t^k$, $s=t^{k+1}$, $a=y_{j-1/2}$, $b=y_{j+1/2}$: setting

  $$Y_{m+1/2}^{\mathrm{Fwd}} = Y(t^{k+1};t^k,y_{m+1/2})$$

  we get

  $$\begin{aligned}
  \bar{g}_m^{k+1} &= \frac{1}{\Delta y}\int_{y_{m-1/2}}^{y_{m+1/2}} g(t^{k+1},z)\,\mathrm{d}z \\
  &= \frac{1}{\Delta y}\int_{Y_{m-1/2}^{\mathrm{Fwd}}}^{Y_{m+1/2}^{\mathrm{Fwd}}} g(t^{k+1},z)\,\mathrm{d}z + \frac{1}{\Delta y}\left(\int_{y_{m-1/2}}^{Y_{m-1/2}^{\mathrm{Fwd}}} g(t^{k+1},z)\,\mathrm{d}z + \int_{Y_{m+1/2}^{\mathrm{Fwd}}}^{y_{m+1/2}} g(t^{k+1},z)\,\mathrm{d}z\right) \\
  &= \frac{1}{\Delta y}\int_{y_{m-1/2}}^{y_{m+1/2}} g(t^k,z)\,\mathrm{d}z - \frac{1}{\Delta y}\left(\int_{y_{m+1/2}}^{Y_{m+1/2}^{\mathrm{Fwd}}} g(t^{k+1},z)\,\mathrm{d}z - \int_{y_{m-1/2}}^{Y_{m-1/2}^{\mathrm{Fwd}}} g(t^{k+1},z)\,\mathrm{d}z\right) \\
  &= \bar{g}_m^k - \frac{\Delta t}{\Delta y}(\bar{G}_{m+1/2}^k - \bar{G}_{m-1/2}^k).
  \end{aligned}$$

  The expression of the flux becomes

  $$\bar{G}_{m+1/2}^k = \frac{1}{\Delta t}\int_{y_{m+1/2}}^{Y_{m+1/2}^{\mathrm{Fwd}}} g(t^{k+1},z)\,\mathrm{d}z = \frac{1}{\Delta t}\Big(\mathscr{G}^{k+1}(Y_{m+1/2}^{\mathrm{Fwd}}) - \mathscr{G}^{k+1}(y_{m+1/2})\Big)$$

  with $\mathscr{G}^{k+1}$ a primitive of $g(t^{k+1},\cdot)$. Mass conservation implies

  $$\mathscr{G}^{k+1}(Y_{m+1/2}^{\mathrm{Fwd}}) = \mathscr{G}^k(y_{m+1/2}) = \sum_{\mu=0}^{m}\bar{g}_\mu^k.$$

  Coming back to the construction of numerical fluxes, we seek a relevant definition of the approximation of $\mathscr{G}^{k+1}(y_{m+1/2})$, while we have a natural formula by means of the g_μ^k's on the Lagrangian interfaces $Y_{m+1/2}^{\mathrm{Fwd}}$. Again this appeals to interpolation procedures.

For our purposes, the Vlasov equation is coupled to a hydrodynamic system. In particular, the characteristics equation for the velocity variable depends on the fluid velocity. For this reason, we adopt the forward framework, using the available fluid velocity u^k to advance in time the characteristics.

Remark 3.1 *Let us precise some formulae in the specific case where D is constant. For* (3.11) *the characteristic equation is*

$$\frac{\mathrm{d}}{\mathrm{d}s}X = v,$$

which yields

$$X(t^2) = X(t^1) + v(t^2 - t^1).$$

Therefore, considering a given discrete velocity v_j, we simply have

$$X^{\mathrm{Back}}_{i+1/2} = x_{i+1/2} - \Delta t v_j, \qquad X^{\mathrm{Fwd}}_{i+1/2} = x_{i+1/2} + \Delta t v_j.$$

Note that the size of the Lagrangian cells $[X^{\mathrm{Back}}_{i-1/2}, X^{\mathrm{Back}}_{i+1/2}]$ (resp. $[X^{\mathrm{Fwd}}_{i-1/2}, X^{\mathrm{Fwd}}_{i+1/2}]$) remains the one of the original mesh Δx. For (3.12)*, we consider*

$$\frac{\mathrm{d}}{\mathrm{d}s}V = D(\bar{u} - V),$$

where $\bar{u}$ is supposed not to depend on time, representing the fluid velocity at given time and position. We get

$$V^{\mathrm{Back}}_{j+1/2} = v_{j+1/2}e^{D\Delta t} + \bar{u}^k_i(1 - e^{D\Delta t}), \qquad V^{\mathrm{Fwd}}_{j+1/2} = v_{j+1/2}e^{-D\Delta t} + \bar{u}^k_i(1 - e^{-D\Delta t}).$$

In particular, the size of the Lagrangian mesh differs from the size of the original mesh:

$$V^{\mathrm{Back}}_{j+1/2} - V^{\mathrm{Back}}_{j-1/2} = e^{+D\Delta t}(v_{j+1/2} - v_{j-1/2}), \qquad V^{\mathrm{Fwd}}_{j+1/2} - V^{\mathrm{Fwd}}_{j-1/2} = e^{-D\Delta t}(v_{j+1/2} - v_{j-1/2}).$$

When D depends on $|v - u|$, the characteristic curves need to be evaluated through a suitable approximation procedure in order to solve the corresponding ODE for V.

3.2 Reconstruction procedure

What is crucial with Semi-Lagrangian methods that can be expressed as a Finite Volume scheme (3.15) is the mass conservation property which is guaranteed by construction. The next ingredient relies on a suitable interpolation procedure in order to define an evaluation of the primitive of the unknown, a quantity which is naturally known only at the cell interfaces (Backward methods) or at the image of the cell interfaces by the Lagrangian flow (Forward methods). Several numerical properties guide the design of the interpolation procedure:

- bearing in mind its physical meaning, the numerical unknown should remain non negative,
- in order to preserve local extrema, the scheme should be non-oscillatory,
- the expected shape of the solution should be preserved, the numerical diffusion should be as reduced as possible,
- and the numerical cost should be as reduced as possible too, both in terms of computational time and memory storage.

A low order interpolation method induces excessive numerical diffusion. With high order schemes, the method should incorporate limiter strategies in order to preserve the maximum principle (at least the positivity of the solution). Global methods that connect all points of the grids, like methods based on splines interpolation, are usually less diffusive. However, local methods that involve neighboring points only are easier to extend to a parallel code [27]. A series of works discuss in details the pros and cons of the different interpolation methods [2, 33, 57].

It turns out that two methods are well adapted to our purposes. On the one hand, the Positive Flux Conservative (PFC) method relies on Newton-like expansion using divided differences. It is coupled to a slope limiter in order to preserve a discrete maximum principle and the positivity of the solution. Classical limiters are TVD, but monotonicity is not guaranteed [64]. A more intricate limiter has been introduced in [63]: it is monotone and preserves local extrema. On the other hand, the PPM scheme introduced by P. Woodward and P. Colella uses a piecewise parabolic reconstruction that incorporates a limiter [25, 24], see also [17]. We shall use the improved version designed in [24] with an intricate limiter involving an approximation of the second order derivative of the unknown. We shall use versions of these schemes which are of third order when the solution does not have high gradients. In what follows they will be referred to as the PFC3-TVD, PFC3-NO (depending on the limiter) and PPM2 schemes, respectively. Note that the reconstruction is based on the primitive of f in the PFC3 methods and on the function f itself for PPM2.

For the sake of concreteness, let us detail how the PFC method works in the Forward framework for the velocity equation (3.12). Since the volume of the cells is not conserved in the v direction, we focus on this direction in the sequel. At second order, the PFC scheme reconstructs the primitive with 3-points stencils, at third order it needs 4 points. We refer the reader to [32] for details on the Backward method. In order to define the flux, we need to define the approximated primitive $v \mapsto \tilde{\mathscr{F}}_i^{k+1}(v)$ from its known value on the Lagrangian grid, namely the points $V^{\mathrm{Fwd}}_{j+1/2}$ (we do not write the index i referring to the space variable, see Remark 3.1 to keep track of the dependance with respect to i through the fluid velocity). Indeed, we bear in mind that $\tilde{\mathscr{F}}_i^{k+1}(V^{\mathrm{Fwd}}_{j+1/2}) = \Delta v \sum_{\mu=0}^{j} f^k_{i,j}$. For the second order reconstruction, we can use the 3 points stencil $(V^{\mathrm{Fwd}}_{j-1/2}, V^{\mathrm{Fwd}}_{j+1/2}, V^{\mathrm{Fwd}}_{j+3/2})$ shown in Figure 1.

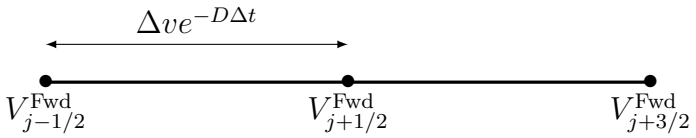

Figure 1: 3 points stencil for the reconstruction.

With the divided differences, we obtain, for $V^{\mathrm{Fwd}}_{j-1/2} \le v \le V^{\mathrm{Fwd}}_{j+1/2}$

$$\tilde{\mathscr{F}}_i^{k+1}(v) = \tilde{\mathscr{F}}_i^{k+1}(V^{\mathrm{Fwd}}_{j+1/2}) + (v - V^{\mathrm{Fwd}}_{j-1/2})\mathrm{dif1c} + \epsilon_{i,j}(v - V^{\mathrm{Fwd}}_{j-1/2})(v - V^{\mathrm{Fwd}}_{j+1/2})\frac{\mathrm{dif1p} - \mathrm{dif1c}}{V^{\mathrm{Fwd}}_{j+3/2} - V^{\mathrm{Fwd}}_{j-1/2}} \tag{3.16}$$

with

$$\mathrm{diflc} = \frac{\tilde{\mathscr{F}}_i^{k+1}(V_{j+1/2}^{\mathrm{Fwd}}) - \tilde{\mathscr{F}}_i^{k+1}(V_{j-1/2}^{\mathrm{Fwd}})}{V_{j+1/2}^{\mathrm{Fwd}} - V_{j-1/2}^{\mathrm{Fwd}}},$$
$$\mathrm{diflp} = \frac{\tilde{\mathscr{F}}_i^{k+1}(V_{j+3/2}^{\mathrm{Fwd}}) - \tilde{\mathscr{F}}_i^{k+1}(V_{j+1/2}^{\mathrm{Fwd}})}{V_{j+3/2}^{\mathrm{Fwd}} - V_{j+1/2}^{\mathrm{Fwd}}}.$$

Note that (3.16) incorporates a slope limiter $0 \le \epsilon_{i,j} \le 1$; its definition will be discussed below. We have

$$\mathrm{dif1c} = e^{D\Delta t} f_{i,j}^k, \qquad \frac{\mathrm{dif1p} - \mathrm{dif1c}}{V_{j+3/2}^{\mathrm{Fwd}} - V_{j-1/2}^{\mathrm{Fwd}}} = \frac{e^{2D\Delta t}(f_{i,j+1}^k - f_{i,j}^k)}{2\Delta v}.$$

Differentiating (3.16), we define a function of the continuous variable v as follows: for $v \in [V_{j-1/2}^{\mathrm{Fwd}}, V_{j+1/2}^{\mathrm{Fwd}}]$:

$$\tilde{f}_i^{k+1}(v) \;\; = e^{D\Delta t} f_{i,j}^n + \epsilon_{i,j}(v - V_j^{\mathrm{Fwd}}) e^{2D\Delta t} \frac{f_{i,j+1}^k - f_{i,j}^k}{\Delta v} \tag{3.17}$$

where $V_j^{\mathrm{Fwd}} = \frac{1}{2}(V_{j-1/2}^{\mathrm{Fwd}} + V_{j+1/2}^{\mathrm{Fwd}})$ is the center of the Lagrangian grid. Of course the update (3.15) is consistent with this expression since $f_{i.j}^{k+1} = \frac{1}{\Delta v}\int_{v_{j-1/2}}^{v_{j+1/2}} \tilde{f}_i^{k+1}(v)\,\mathrm{d}v$. Bearing in mind $|v - V_j^{\mathrm{Fwd}}| \le \frac{1}{2}\Delta v e^{-D\Delta t}$, see Remark 3.1, the slope limiter is defined as follows

$$\epsilon_{i,j} = \begin{cases} \min\left(1, 2\dfrac{f_{i,j}^k - f_{\min_{i,j}}}{f_{i,j+1}^k - f_{i,j}^k}\right) & \text{if } f_{i,j+1}^k - f_{i,j}^k > 0, \\ \min\left(1, -2\dfrac{f_{\max_{i,j}} - f_{i,j}^k}{f_{i,j+1}^k - f_{i,j}^k}\right) & \text{otherwise.} \end{cases}$$

We can rewrite $2\frac{f_{i,j}^k - f_{\min_{i,j}}}{f_{i,j+1}^k - f_{i,j}^k} = 2\frac{\mathrm{dif1c} - e^{D\Delta t} f_{\min_{i,j}}}{\mathrm{dif1p} - \mathrm{dif1c}}$. It is natural to set $f_{\min_{i,j}} = \min(f_{i,j-1}, f_{i,j}, f_{i,j+1})$ and $f_{\max_{i,j}} = \max(f_{i,j-1}, f_{i,j}, f_{i,j+1})$. Indeed, CFL conditions needed for the stability of the numerical scheme ensure that the edges do not cross and so it is efficient to consider the 3 neighboring cells to define a local extremum. The corresponding scheme is TVD, but spurious local extrema can be generated, see [63]. A more intricate definition of $f_{\min}$, $f_{\max}$ leads to a scheme with better abilities in detecting extrema and discontinuities, [64, 63].

The method PFC-3 is based on the same principles but it uses a stencil with 4 points. For the sake of completeness, let us detail the necessary formulae. For $v \in [V_{j-1/2}^{\mathrm{Fwd}}, V_{j+1/2}^{\mathrm{Fwd}}]$, the reconstructed primitive reads:

$$\begin{aligned} \tilde{\mathscr{F}}_i^{k+1}(v) \;\; = \;\; & \tilde{\mathscr{F}}_{i-1/2}^{k+1} + \mathrm{dif1c}(v - V_{j-1/2}^{\mathrm{Fwd}}) + \epsilon_{i,j}^{+} \frac{\mathrm{dif1p} - \mathrm{dif1c}}{v_{j+3/2}^{n+1} - v_{j-1/2}^{n+1}} (v - V_{j-1/2}^{\mathrm{Fwd}})(v - V_{j-+1/2}^{\mathrm{Fwd}}) \\ & + (\epsilon_{i,j}^{+} - \epsilon_{i,j}^{-}) \frac{1}{V_{j+3/2}^{\mathrm{Fwd}} - V_{j-3/2}^{\mathrm{Fwd}}} \left(\frac{\mathrm{dif1p} - \mathrm{dif1c}}{V_{j+3/2}^{\mathrm{Fwd}} - V_{j-1/2}^{\mathrm{Fwd}}} - \frac{\mathrm{dif1c} - \mathrm{dif1m}}{V_{j+1/2}^{\mathrm{Fwd}} - V_{j-3/2}^{\mathrm{Fwd}}} \right) \\ & \qquad \times (v - V_{j-1/2}^{\mathrm{Fwd}})(v - V_{j+1/2}^{\mathrm{Fwd}})(v - V_{j+3/2}^{\mathrm{Fwd}}), \end{aligned}$$

Remarking that $(v - V_{j+3/2}^{\mathrm{Fwd}} + 3\Delta v e^{-D\Delta t}) = v - V_{j-3/2}^{\mathrm{Fwd}}$, we rearrange as follows

$$\begin{aligned}\tilde{\mathscr{F}}_i^{k+1}(v) &= \tilde{\mathscr{F}}_{i-1/2}^{k+1} + \mathrm{dif1c}(v - V_{j-1/2}^{\mathrm{Fwd}}) \\ &\quad + \epsilon_{i,j}^{+} \frac{\mathrm{dif1p} - \mathrm{dif1c}}{6(\Delta v)^2 e^{-2D\Delta t}} \Big((v - V_{j-1/2}^{\mathrm{Fwd}})(v - V_{j+1/2}^{\mathrm{Fwd}})(v - V_{j-3/2}^{\mathrm{Fwd}}) \Big) \\ &\quad - \epsilon_{i,j}^{-} \frac{\mathrm{dif1c} - \mathrm{dif1m}}{6(\Delta v)^2 e^{-2D\Delta t}} \Big((v - V_{j-1/2}^{\mathrm{Fwd}})(v - V_{j+1/2}^{\mathrm{Fwd}})(v - V_{j+3/2}^{\mathrm{Fwd}}) \Big).\end{aligned}$$

Differentiating yields

$$\begin{aligned}\tilde{f}_i^{k+1}(v) &= \mathrm{dif1c} \\ &\quad + \epsilon_{i,j}^{+} \frac{\mathrm{dif1p} - \mathrm{dif1c}}{6(\Delta v e^{-D\Delta t})^2} \Big(2(v - V_j^{\mathrm{Fwd}})(v - V_{j-3/2}^{\mathrm{Fwd}}) + (v - V_{j-1/2}^{\mathrm{Fwd}})(v - V_{j+1/2}^{\mathrm{Fwd}}) \Big) \\ &\quad - \epsilon_{i,j}^{-} \frac{\mathrm{dif1c} - \mathrm{dif1m}}{6(\Delta v e^{-D\Delta t})^2} \Big(2(v - V_j^{\mathrm{Fwd}})(v - V_{j+3/2}^{\mathrm{Fwd}}) + (v - V_{j-1/2}^{\mathrm{Fwd}})(v - V_{j+1/2}^{\mathrm{Fwd}}) \Big).\end{aligned}$$

The limiters are then defined by

$$\epsilon_{i,j}^{+} = \begin{cases} \min\left(1, 2\dfrac{f_{i,j}^k - f_{\min_{i,j}}}{f_{i,j+1}^k - f_{i,j}^k}\right) & \text{if } f_{i,j+1}^k - f_{i,j}^k > 0, \\ \min\left(1, -2\dfrac{f_{\max_{i,j}} - f_{i,j}^k}{f_{i,j+1}^k - f_{i,j}^k}\right) & \text{otherwise,} \end{cases}$$

and

$$\epsilon_{i,j}^{-} = \begin{cases} \min\left(1, 2\dfrac{f_{\max_{i,j}} - f_{i,j}^k}{f_{i,j}^k - f_{i,j-1}^k}\right) & \text{if } f_{i,j+1}^k - f_{i,j}^k > 0, \\ \min\left(1, -2\dfrac{f_{i,j}^k - f_{\min_{i,j}}}{f_{i,j}^k - f_{i,j-1}^k}\right) & \text{otherwise.} \end{cases}$$

Remark 3.2 *It is worth pointing out that in practice we do not need to evaluate the function $\tilde{f}_i(v)$: only the primitive $\tilde{\mathscr{F}}_i(v)$ enters in the definition of the Finite Volume scheme.*

To complete the discussion, let us present a few numerical results for the simple homogeneous case

$$\partial_t f + \partial_v(-D(v-u)f) = 0. \tag{3.18}$$

with a given constant gas velocity u. We bear in mind that the solution satisfies

$$\min f(0,v) e^{Dt} \le f(t,v) \le \max f(0,v) e^{Dt}. \tag{3.19}$$

Since the particle distribution function is space-homogeneous and u is constant, the macroscopic density does not change ($\partial_t n = 0$) while the current is explicitly given by

$$J(t) = \int v f(t,v)\,\mathrm{d}v = J(0)e^{-Dt} + nu(1 - e^{-Dt}), \tag{3.20}$$

Similarly, we can find an explicit expression for the kinetic energy $K(t)$. We compare the performances of the Semi-Lagrangian methods PPM2 and PFC3. For the simulation, we

work with dimensionless quantities and we set $u = 0.15$ and $n = 0.2$. The drag coefficient is $D = 1$. The initial distribution function is a staircase function such that $J(0) = -0.14$. Due to the drag force the velocities of the particles relax to a common value, the gas velocity. We run the code with $N_v = 200$, $N_v = 400$ and $N_v = 800$. The evolution of the current is represented in Fig. 2; the error can be found in Fig. 3. The error to the exact solution remains small (of the order of 10^{-3} with $N_v = 200$, 10^{-4} with $Nv = 400$ and with $Nv = 800$). For short times of simulation, PFC3-NO has the smallest error (the PFC3-NO limiter outperforms the PFC3-TVD limiter), but for longer times, PPM2 becomes better.

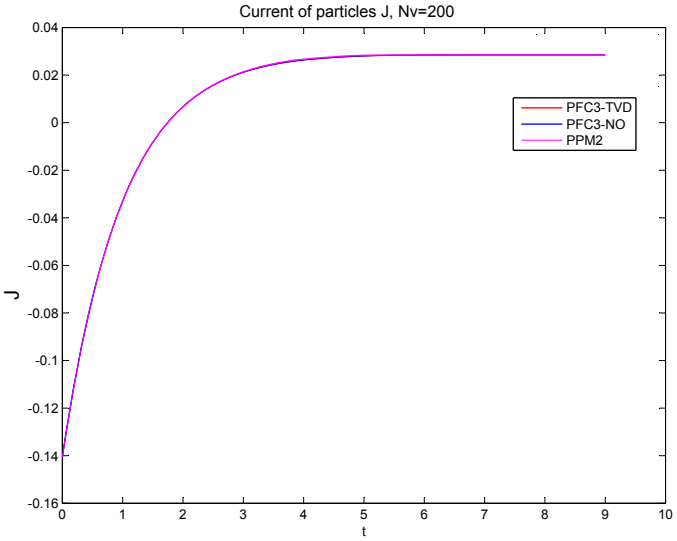

Figure 2: Time-evolution of the current $t \mapsto J(t)$ for the homogeneous problem (3.18). The schemes PFC3-TVD , PFC3-NO and PPM2 produce very similar results.

The shape of the distribution function can be more or less altered depending on the method. Results are presented in Fig. 4-6 where $N_v = 400$. Besides, we compare to the exact distribution function at each time (the staircase profile is simply advected and dilated according to (2.6)) and with the numerical solution produced by a second order MUSCL scheme. The scheme PFC3-TVD diffuses the jumps, while the PFC3-NO limiter preserves the extrema with a better accuracy. The scheme PPM2 presents a better shape of the solution, with sensible advantage for longer times of simulation. In all cases the Semi-Lagrangian method clearly outperforms MUSCL. Already with $N_v = 200$ the numerical current J is acceptable, while the quality of the particle distribution function is greatly improved with a higher number of points of discretisation (see Fig. 7-9 with $N_v = 800$) especially for the longer times. In order to reduce overshoots, PPM2 needs a quite refined mesh. We point out that reproducing precisely the shape of a discontinuous distribution function is not the primary objective for our purposes. Instead, having an accurate approximation of the moments is needed due to the coupling in the drag source term of the fluid equation.

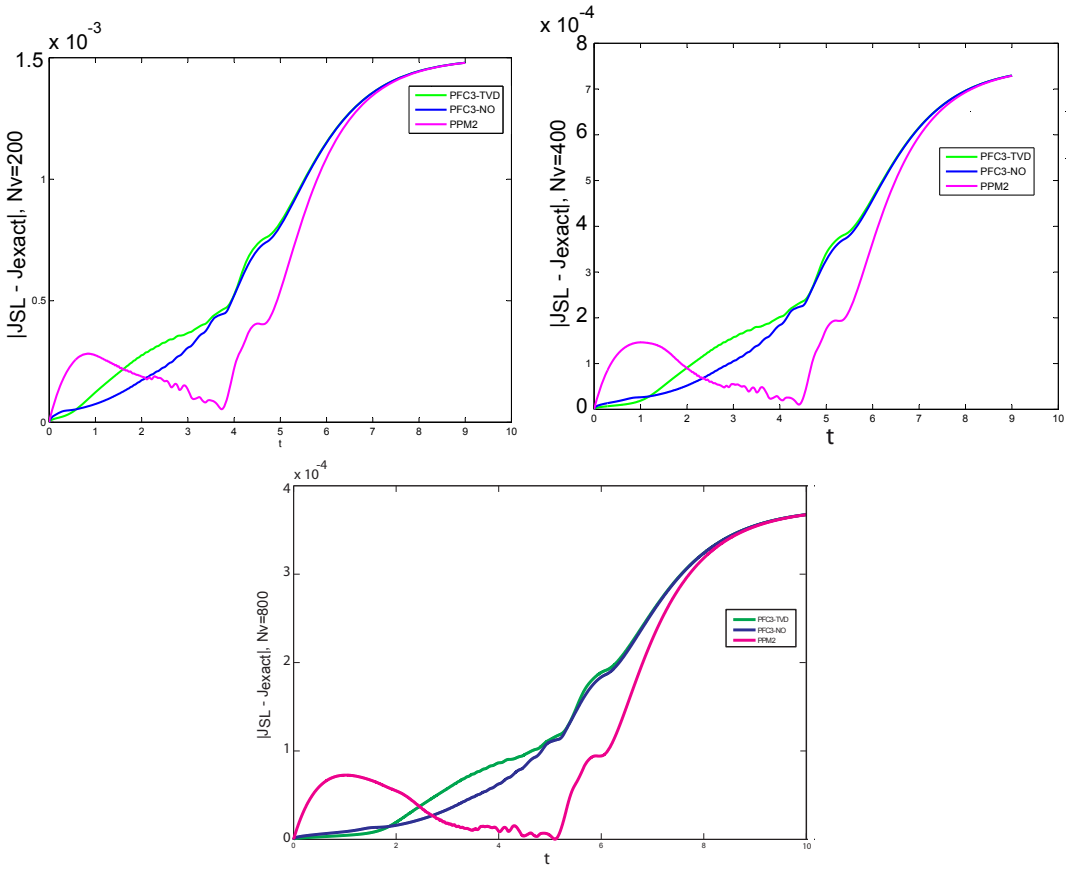

Figure 3: Simulation of the homogeneous problem (3.18): Absolute error between the numerical Semi-Lagrangian scheme PFC3 or PPM2 and the exact solutions $J(t)$ with $N_v = 200$ (top left), $N_v = 400$ (top right), $N_v = 800$ (bottom).

4 Treatment of the coupling: time–splitting, space discretization and source terms

We are going to use a time splitting with a predictor-corrector strategy in order to treat the fluid-particle system. A difficulty is specifically related to the technical constraint on the treatment of the hydrodynamic equations: we shall use staggered grids where the density and pressure are evaluated at the centers of the cells while the velocity is stored on the cell interfaces. This choice is due to the fact that for the applications of interest, the hydrodynamic is treated with the BBC scheme [68]. We will present several options to handle the coupling and in particular for the discrete expression of the source coupling terms. We start with the simple case where the fluid system reduces to the Burgers equation. Then, we extend the scheme with the isentropic Euler system.

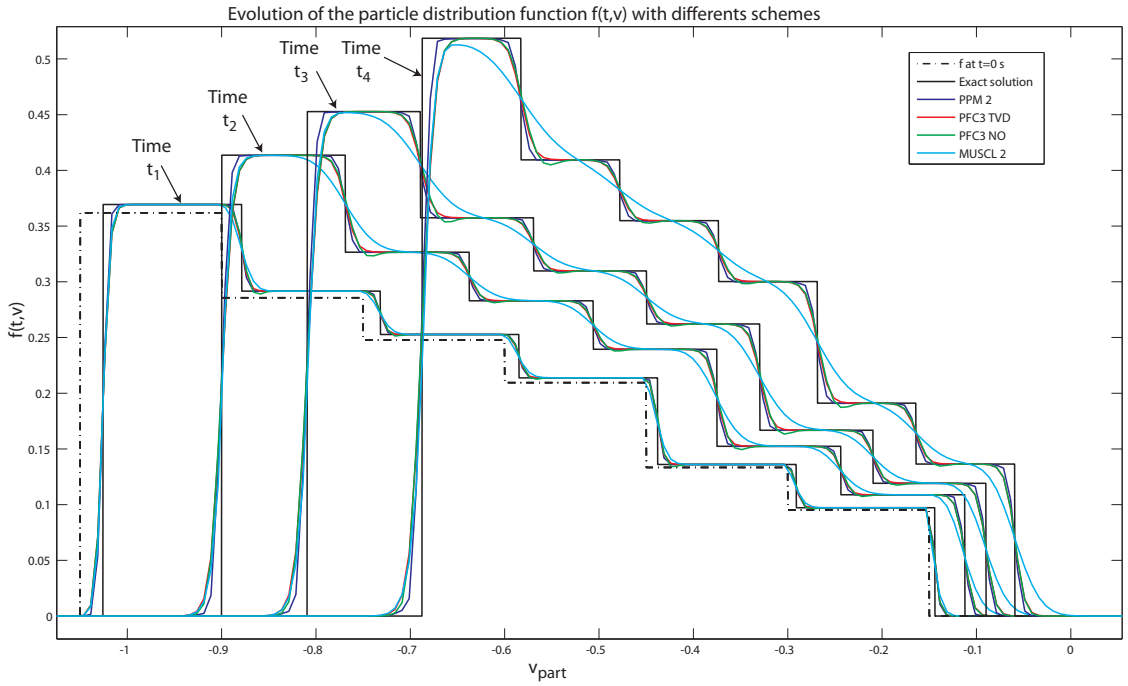

Figure 4: Simulation of the homogeneous problem (3.18): Particle distribution function at time $t_1 = 0.02$ s, $t_2 = 0.13$ s, $t_3 = 0.22$ s, $t_4 = 0.36$ s with the PFC3-TVD , PFC3-NO, PPM2 and second order MUSCL numerical schemes, comparison with the exact solution, $N_v = 400$.

4.1 Vlasov–Burgers system

We consider the system

$$\begin{aligned} &\partial_t f + \partial_x(vf) + \partial_v(D(u-v)f) = 0, \\ &\partial_t u + \partial_x(u^2/2) = S, \\ &S(t,x) = \tfrac{m_{\mathrm{d}}}{\varrho_{\mathrm{f}}} \int D(v-u(t,x))f(t,x,v)\,\mathrm{d}v. \end{aligned} \tag{4.21}$$

Let us describe how the scheme works. We have at hand at time t^k the discrete particle distribution function $f_{i.j}^k$ and the fluid velocity $u_{i+1/2}^k$, the later being stored at the interfaces $x_{i+1/2}$ of the space grid.

4.2 Time-splitting: prediction–correction strategy

To update these quantities we proceed as follows.

- *Step 1.1: Prediction of the fluid velocity.*

  We find $u_{i+1/2}^{k+1/2}$ by using the Finite Volume scheme

$$u_{i+1/2}^{k+1/2} = u_{i+1/2}^k - \frac{\Delta t}{2\Delta x}(G_{i+1}^k - G_i^k) + \frac{\Delta t}{2} S_{i+1/2}^k. \tag{4.22}$$

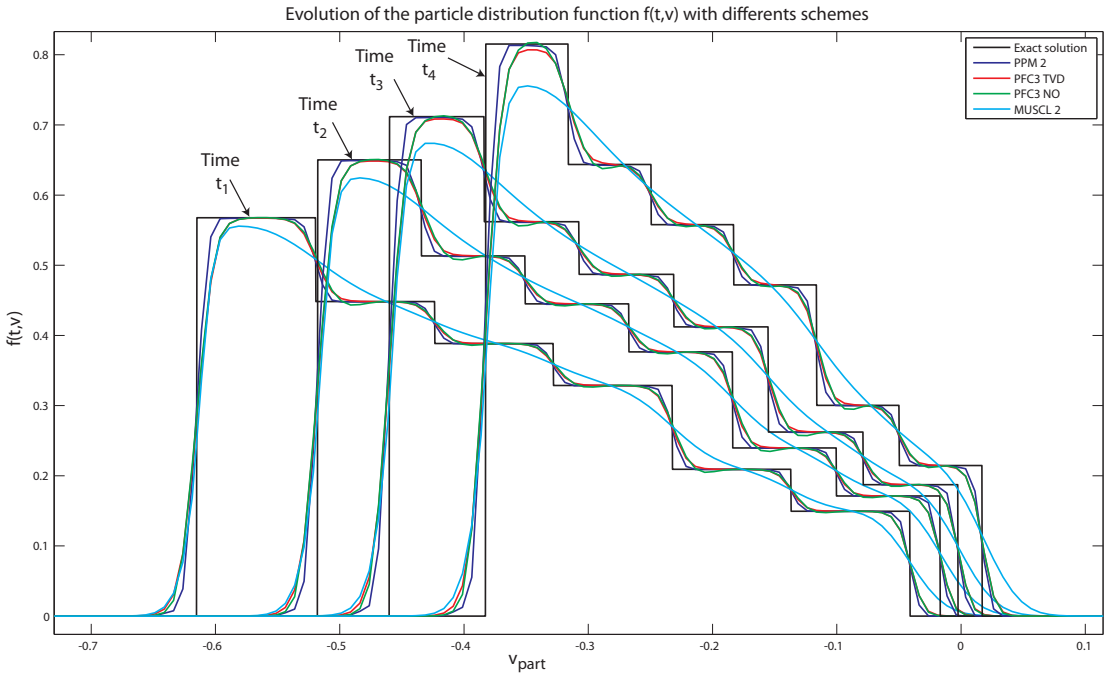

Figure 5: Simulation of the homogeneous problem (3.18): Particle distribution function at time $t_1 = 0.45$ s, $t_2 = 0.58$ s, $t_3 = 0.67$ s, $t_4 = 0.75$ s with the PFC3-TVD , PFC3-NO, PPM2 and second order MUSCL numerical schemes, comparison with the exact solution, $N_v = 400$.

Here, G^k_{i+1} is a certain numerical flux, a function of the discrete velocities on a set of neighboring cells $u^k_{i-\mu+1/2}, ..., u^k_{i+\mu+1/2}$ (for instance the Engquist-Osher flux [31], which is expressed as $g(u,v) = \frac{u(u+|u|)}{4} + \frac{v(v-|v|)}{4}$ for the Burgers equation). For our simulation we use a standard MUSCL scheme which reaches the second order accuracy (for smooth solutions). The source term $S^n_{i+1/2}$ is a suitable discretization of the drag force term at the interface $i + 1/2$. This point will be detailed below.

- *Step 1.2: Prediction of the particle distribution function.*

  We make use of the directional splitting "xvx", written in the Strang fashion, as it is usual in plasma physics.

  Step 1.2.1:Transport with velocity v in the direction x.

  We solve (3.11) on the time step $\frac{\Delta t}{4}$. We use the Finite Volume Semi-Lagrangian strategy described above for each v_j, the particle velocity at the center of the cell i, j; it gives

  $$f^*_{i,j} = f^k_{i,j} - \frac{\Delta t}{4\Delta x}(F^k_{i+1/2,j} - F^k_{i-1/2,j}). \tag{4.23}$$

  Step 1.2.2: Equation with the drag force in the direction v.

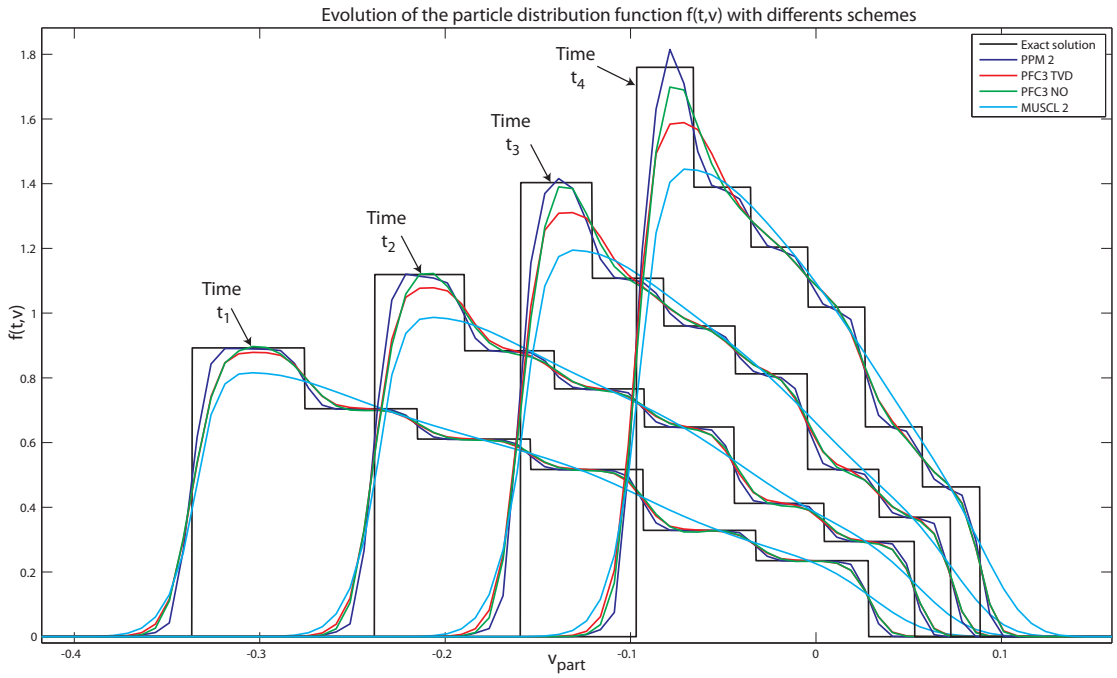

Figure 6: Simulation of the homogeneous problem (3.18): Particle distribution function at time $t_1 = 0.90$ s, $t_2 = 1.13$ s, $t_3 = 1.36$ s, $t_4 = 1.58$ s with the PFC3-TVD , PFC3-NO, PPM2 and second order MUSCL numerical schemes, comparison with the exact solution, $N_v = 400$.

We solve (3.12) on the time step $\frac{\Delta t}{2}$. The equation is considered as an uncoupled set of space homogeneous problems, with a constant fluid velocity

$$u_i^k = \frac{u_{i-1/2}^k + u_{i+1/2}^k}{2}.$$

The updating can be written in the Finite Volume fashion

$$f_{i,j}^{**} = f_{i,j}^{*} - \frac{\Delta t}{2\Delta v}(F_{i,j+1/2}^{*} - F_{i,j-1/2}^{*}). \tag{4.24}$$

Note that the discrete density $f_{i,j}^{*}$ coming from the previous step is used in all terms of the right hand side.

Step 1.2.3: Transport with velocity v in the direction x.

We go back to (3.11) for a time step $\frac{\Delta t}{4}$; in (4.23) we replace $f_{i.j}^{k}$ by $f_{i.j}^{**}$ both in the initial data term and in the definition of the numerical fluxes.

We have now determined a prediction of all the unknowns $u_{i+1/2}^{k+1/2}$ and $f_{i,j}^{k+1/2}$. We shall use these quantities to compute new fluxes and source terms.

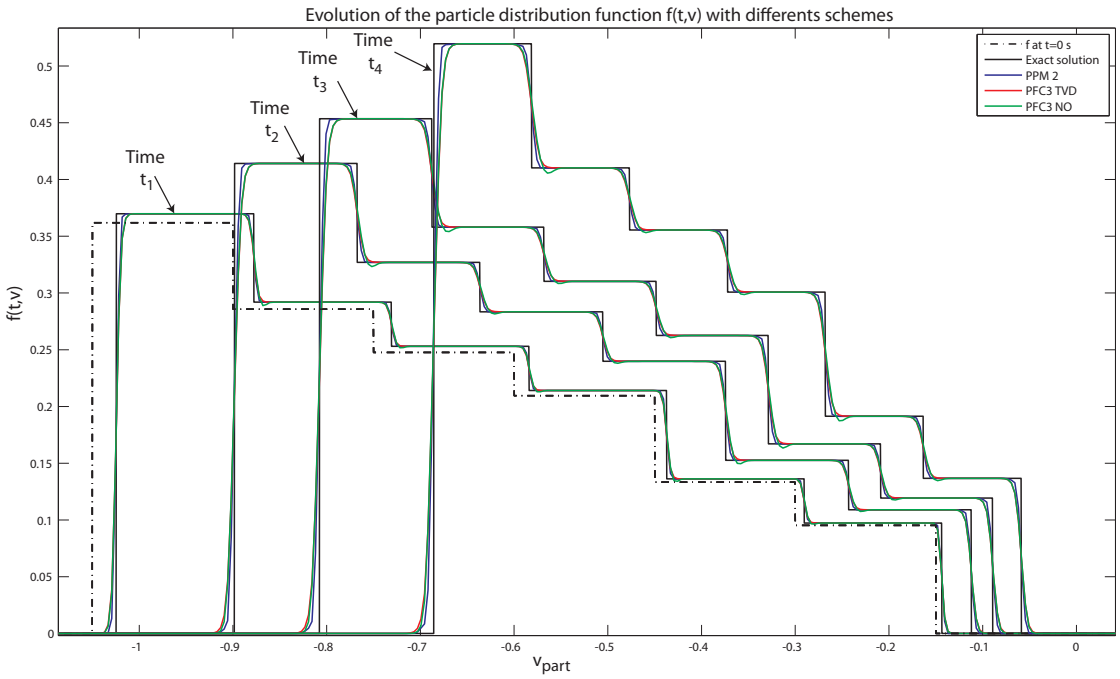

Figure 7: Simulation of the homogeneous problem (3.18): Particle distribution function at time $t_1 = 0.02$ s, $t_2 = 0.13$ s, $t_3 = 0.22$ s, $t_4 = 0.36$ s with the PFC3-TVD , PFC3-NO, PPM2 numerical schemes, comparison with the exact solution, $N_v = 800$.

- *Step 2.1: Correction of the fluid velocity.*

  We solve the Burgers equation on the time interval (t^k, t^{k+1}) with

$$u_{i+1/2}^{k+1} = u_{i+1/2}^{k} - \frac{\Delta t}{\Delta x}(G_{i+1}^{k+1/2} - G_{i}^{k+1/2}) + \Delta t S_{i+1/2}^{k+1/2}. \tag{4.25}$$

  The numerical fluxes and the source terms are defined by using the predicted quantities $u_{i+1/2}^{k+1/2}$ and $f_{i,j}^{k+1/2}$.

- *Step 2.2: Correction of the particle distribution function.*

  We solve the Vlasov equation on the time interval (t^k, t^{k+1}). We use the same Strang splitting as in Steps 1.2.1 to 1.2.3; it reads

$$f_{i,j}^{*} = f_{i,j}^{n} - \frac{\Delta t}{2\Delta x}(F_{i+1/2,j}^{k+1/2} - F_{i-1/2,j}^{k+1/2}), \tag{4.26}$$

$$f_{i,j}^{**} = f_{i,j}^{*} - \frac{\Delta t}{\Delta v}(F_{i,j+1/2}^{*} - F_{i,j-1/2}^{*}), \tag{4.27}$$

$$f_{i,j}^{k+1} = f_{i,j}^{**} - \frac{\Delta t}{2\Delta x}(F_{i+1/2,j}^{**} - F_{i-1/2,j}^{**}), \tag{4.28}$$

  By contrast to a standard prediction-correction approach, we point out that in the definition of the fluxes in (4.26), we use the velocity $u_i^{k+1/2} = \frac{u_{i+1/2}^{k+1/2} + u_{i-1/2}^{k+1/2}}{2}$ but this is

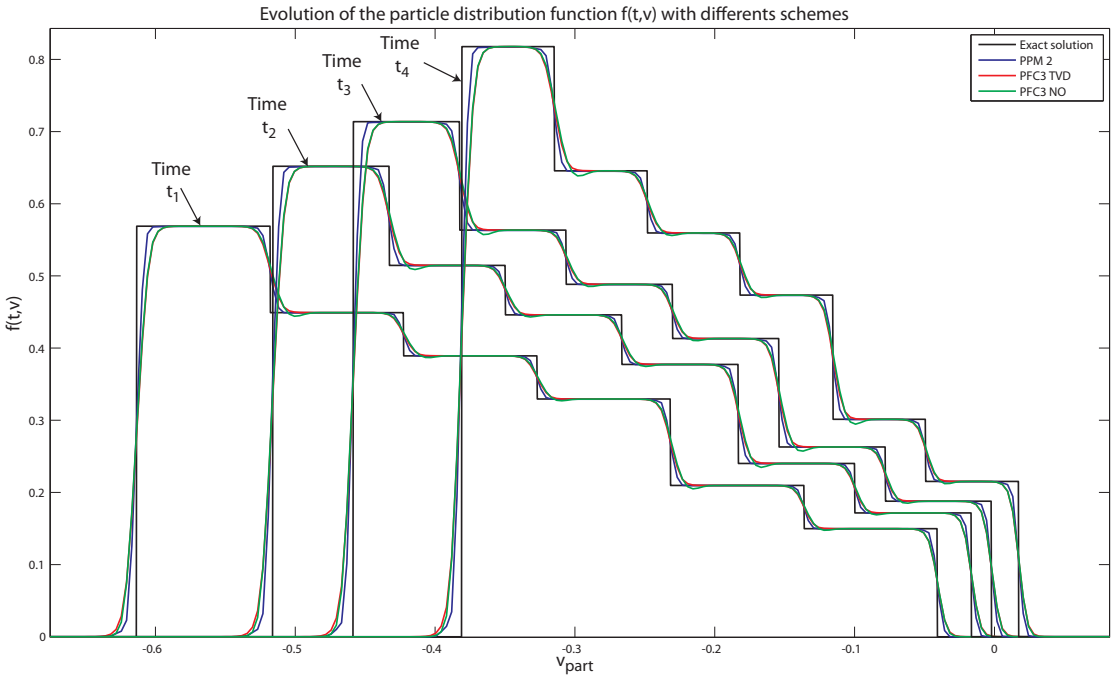

Figure 8: Simulation of the homogeneous problem (3.18): Particle distribution function at time $t_1 = 0.45$ s, $t_2 = 0.58$ s, $t_3 = 0.67$ s, $t_4 = 0.75$ s with the PFC3-TVD , PFC3-NO, PPM2 numerical schemes, comparison with the exact solution, $N_v = 800$.

the distribution function $f_{i,j}^k$ which enters into the definition of $F_{i+1/2,j}^{k+1/2}$. (Using $f_{i,j}^{k+1/2}$ does not respect (2.8) and definitely alters the numerical results.) These procedures define $u_{i+1/2}^{k+1}$ and $f_{i,j}^{k+1}$. We obtain the macroscopic quantities, stored on the nodes x_i's, by velocity averaging

$$n_i^{k+1} = \Delta v \sum_j f_{i,j}^{k+1}, \qquad J_i^{k+1} = \Delta v \sum_j v_j f_{i,j}^{k+1}.$$

4.3 Comments on the time step

A complete stability analysis of the scheme is beyond the scope of the present work. Nevertheless, we can identify several sources for restricting the time step. First of all, the usual CFL condition for the Burgers equation (without source term) reads

$$\max_i(|u_{i+1/2}^k|)\Delta t_1 \leq \Delta x. \tag{4.29}$$

Next, the source term induces further restriction: considering the ODE $\partial_t u = \frac{m_\mathrm{d}}{\varrho_\mathrm{f}} D(J - nu)$, yields

$$\Delta t_2 < \frac{\varrho_\mathrm{f}}{D m_\mathrm{d} n}, \tag{4.30}$$

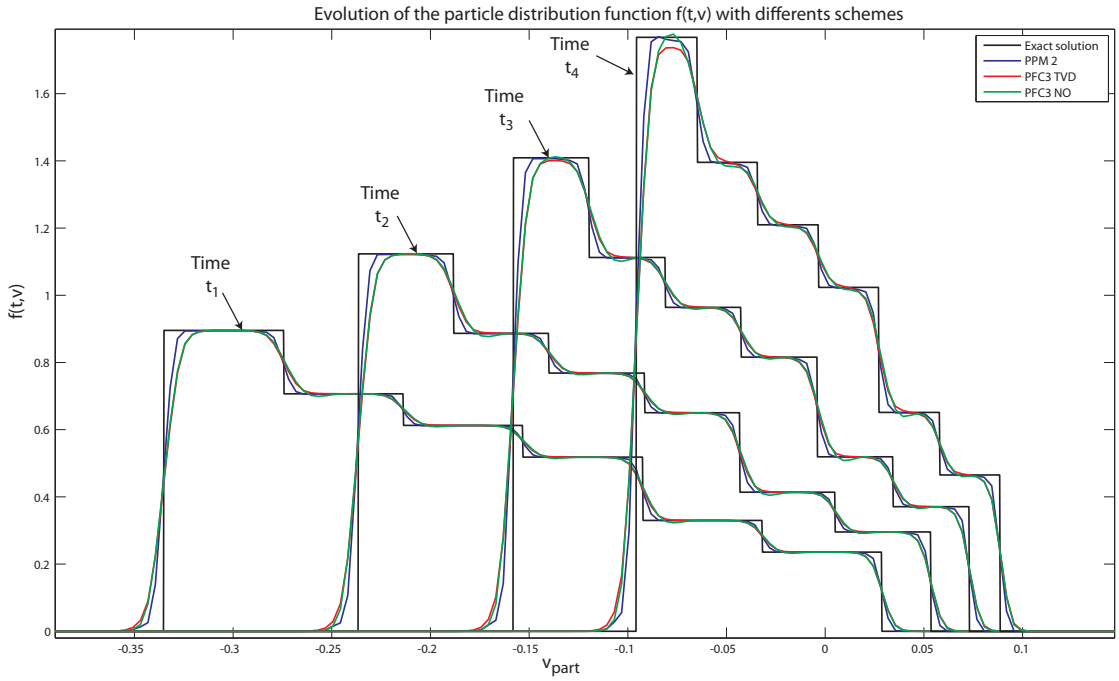

Figure 9: Simulation of the homogeneous problem (3.18): Particle distribution function at time $t_1 = 0.90$ s, $t_2 = 1.13$ s, $t_3 = 1.36$ s, $t_4 = 1.58$ s with the PFC3-TVD , PFC3-NO, PPM2 numerical schemes, comparison with the exact solution, $N_v = 800$.

Clearly, it becomes a strong restriction in high friction regimes $D \gg 1$. It is likely that it can be improved by using some tricky implicit version of the algorithm, see e.g. for the design of such schemes able to handle asymptotic problems [22, 40]. Finally, (3.11) and (3.12) also leads to restrictions on the time step that read

$$\max(|v|)\Delta t_3 \leq \Delta x, \tag{4.31}$$

$$\max(D|v-u|)\Delta t_4 \leq \Delta v, \tag{4.32}$$

in order to avoid the crossing of the characteristics during a time step. In practice, we replace (4.32) by

$$\Delta t_4 \leq \frac{\Delta v}{D(\max_j(|v_j|) + \max_i(|u_i|))}. \tag{4.33}$$

Eventually, the time step is determined by $\Delta t = \mathrm{CFL}\min(\Delta t_1, \Delta t_2, \Delta t_3, \Delta t_4)$, where we set $\mathrm{CFL} = 0.5$. It is worth pointing out that (4.31) and (4.32) imply that the Lagrangian cells do not move beyond half a cell of the space or velocity mesh, and thus the characteristics emanating from interfaces do not intersect.

4.4 Source term

Since we have decided to work on a staggered grid for the fluid velocity, there is a difficulty in defining the discrete source terms $S^k_{i+1/2}$, $S^{k+1/2}_{i+1/2}$ for (4.22) and (4.25) respectively. We

bear in mind that the source term involves both the particle distribution function, known on the cell centers x_i, and the fluid velocity, associated to the interfaces $x_{i+1/2}$. Let us discuss several options:

- We have at hand the macroscopic density n_i^k and the current J_i^k stored at the center of the cells. The simplest solution consists in defining the value at the interface $x_{i+1/2} = \frac{x_i+x_{i+1}}{2}$ by the mean value $n_{i+1/2}^k = \frac{n_i^k+n_{i+1}^k}{2}$, $J_{i+1/2}^k = \frac{J_i^k+J_{i+1}^k}{2}$ so that $S_{i+1/2}^k = \frac{m_\mathrm{d}}{\varrho_\mathrm{f}} D(J_{i+1/2}^k - \rho_{i+1/2}^j u_{i+1/2}^k)$. General source terms can be defined similarly by using the mean value of the distribution function $f_{i+1/2,j}^k = \frac{f_{i,j}^k+f_{i+1,j}^k}{2}$.

- Following [57], we can define n and J directly on the interface at the end of the steps that solve the transport in the x direction (3.11). The motivation relies on the discrete version of the mass conservation (2.7), which reads

$$n_i^{k+1} = n_i^k - \frac{\Delta t}{\Delta x}\Big(J_{i+1/2}^k - J_{i-1/2}^k\Big). \tag{4.34}$$

  Summing (4.26), (4.27) and (4.28) over velocities provides the following definition of the current on the interface $x_{i+1/2}$:

$$J_{i+1/2}^k = \frac{\Delta v}{2}\sum_{j=1}^{N_v}(F_{i+1/2,j}^k + F_{i+1/2,j}^{**}). \tag{4.35}$$

  For the density, we can use either $n_{i+1/2}^k = \Delta v \sum_{j=1}^{N_v} \frac{(F_{i+1/2,j}^k + F_{i+1/2,j}^{**})}{2v_j}\mathbf{1}_{v_j\neq 0}$ (observe that for $v_j = 0$, the flux $F_{i+1/2,j}$ vanishes since the interface $x_{i+1/2}$ does not move) or the simple mean $n_{i+1/2}^k = \frac{n_i^k+n_{i+1}^k}{2}$. This approach is well-adapted when the drag force depends linearly on the relative velocity because in this situation the right hand side of the hydrodynamic equation is directly defined by the macroscopic quantities n and J. However, it does not apply to cases where D depends on $|v-u|$: the force exerted by the particles on the fluid $\int D(|v-u|)(v-u)f\,\mathrm{d}v$ cannot be expressed by means of n and J.

- Finally, we can also use the numerical fluxes involved in the resolution of (3.12). The idea relies on the following identity which holds for the continuous problem

$$\frac{m_\mathrm{d}}{\varrho_\mathrm{f}}\int v\partial_v(D(u-v)f)\,\mathrm{d}v = +\frac{m_\mathrm{d}}{\varrho_\mathrm{f}}\int D(v-u)f\,\mathrm{d}v = S.$$

  Therefore by considering the first order moment in (4.24), we obtain

$$\Delta v\sum_{j=1}^{N_v} v_j f_{i,j}^{**} = \Delta v\sum_{j=1}^{N_v} v_j f_{i,j}^{*} - \Delta t\sum_{j=1}^{N_v} v_j\Big(F_{i,j+1/2}^{*} - F_{i,j-1/2}^{*}\Big). \tag{4.36}$$

  Integrating by parts, it can be rewritten as

$$J_i^{**} = J_i^{*} + \Delta t\Delta v\sum_{j=1}^{N_v-1} F_{i,j+1/2}^{*} - \Delta t\Big[v_{Nv}F_{i,Nv+1/2}^{*} - v_1 F_{i,1/2}^{*}\Big]. \tag{4.37}$$

It yields the following definition of the source term, evaluated at the center of the cell

$$S_i = -\Delta v \frac{m_\mathrm{d}}{\varrho_\mathrm{f}} \sum_{j=1}^{N_v-1} F_{i,j+1/2} + \Delta t \frac{m_\mathrm{d}}{\varrho_\mathrm{f}} \Big[F_{i,Nv+1/2} v_{N_v} - F_{i,1/2} v_1 \Big]. \tag{4.38}$$

Due to the splitting "xvx" this approach does not take into account the last step of the directional splitting. It would be better adapted with the "vxv" splitting. The source term at the interface can then be defined by the mean value $S^n_{i+1/2} = \frac{S^n_i + S^n_{i+1}}{2}$.

In order to improve the performances of the scheme, in particular for high friction regimes, it might be appealling to use upwinding techniques in the treatment of the source term. We refer the reader to [10, 37], for the design of such method for scalar hyperbolic equations, to [11] for systems, and to the complete overview in [36]. The standard scheme reads

$$\frac{\Delta x}{\Delta t}(u^{k+1}_{i+1/2} - u^k_{i+1/2}) + G^k_{i+1} - G^k_i = \Delta x S^k_{i+1/2} \tag{4.39}$$

with a suitable numerical flux defined as a function of the neighboring numerical unknowns

$$G^k_{i+1} = \mathbf{G}(u^k_{i+3/2}, u^k_{i+1/2}), \qquad G^k_i = \mathbf{G}(u^k_{i+1/2}, u^k_{i-1/2}).$$

The idea consists in embodying the source term into the numerical flux, through the definition of suitable auxiliary numerical unknowns $u^{k,-}_{i+3/2}$, $u^{k,+}_{i-1/2}$. Then, (4.39) is replaced by

$$\frac{\Delta x}{\Delta t}(u^{k+1}_{i+1/2} - u^k_{i+1/2}) + \tilde{G}^k_{i+1} - \tilde{G}^k_i = 0 \tag{4.40}$$

with

$$\tilde{G}^k_{i+1} = \mathbf{G}(u^{k,-}_{i+3/2}, u^k_{i+1/2}), \qquad \tilde{G}^k_i = \mathbf{G}(u^k_{i+1/2}, u^{k,+}_{i-1/2}).$$

Note that we can equivalently write

$$\frac{\Delta x}{\Delta t}(u^{k+1}_{i+1/2} - u^k_{i+1/2}) + G^k_{i+1} - G^k_i = \Delta x \tilde{S}^k_{i+1/2} \tag{4.41}$$

with

$$\Delta x \tilde{S}^k_{i+1/2} = (G^k_{i+1} - \tilde{G}^k_{i+1}) - (G^k_i - \tilde{G}^k_i). \tag{4.42}$$

The idea consists in solving the stationary equation

$$\partial_x(u^2/2) = S = \frac{m_\mathrm{d}}{\varrho_\mathrm{f}} D(J - nu) \tag{4.43}$$

on a space step. From the known values $u^k_{i+3/2}, u^k_{i-1/2}$ we define this way two quantities $u^{k,-}_{i+3/2}$ and $u^{k,+}_{i-1/2}$ which can be used in the definition of the numerical fluxes and source terms. To be more specific, we proceed as follows. Equation (4.43) can be rewritten as

$$\frac{\mathrm{d}}{\mathrm{d}x}\left(-\frac{J}{n^2} \ln(|J - nu|) - \frac{u}{n} \right) = \frac{m_\mathrm{d}}{\varrho_\mathrm{f}} D.$$

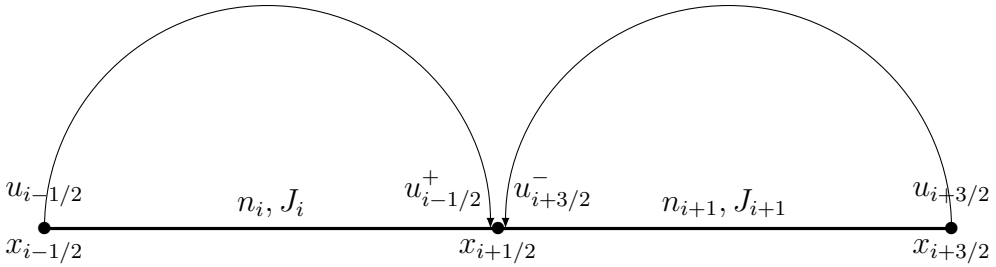

Figure 10: Resolution of two stationary problems for the edge $i+1/2$, on the left cell i to get $u^+_{i-1/2}$ from $u_{i-1/2}$ and on the right cell $i+1$ to get $u^-_{i+3/2}$ from $u_{i+3/2}$.

We integrate "backward" on $I_{i+1} = [x_{i+1/2}, x_{i+3/2}]$ and "forward" on $I_i = [x_{i-1/2}, x_{i+1/2}]$, respectively (see Fig. 10).

In this computation, since the discrete particle density n and current J are stored on the grid points x_i, we naturally set

$$\Phi_i(u) = \frac{J_i}{n_i^2}\ln(|J_i - n_i u|) + \frac{u}{n_i}.$$

Hence, we get

$$\Phi_i(u^{k,+}_{i-1/2}) = \Phi_i(u^k_{i-1/2}) - \frac{m_{\rm d}}{\varrho_{\rm f}} D\Delta x, \qquad \Phi_{i+1}(u^{k,-}_{i+3/2}) = \Phi_{i+1}(u^k_{i+3/2}) + \frac{m_{\rm d}}{\varrho_{\rm f}} D\Delta x.$$

We obtain

$$\ln\left(\left|1 - \frac{n^k_{i+1}u^{k,-}_{i+3/2}}{J^k_{i+1}}\right|\right) + \frac{n^k_{i+1}u^{k,-}_{i+3/2}}{J^k_{i+1}} = \ln\left(\left|1 - \frac{n^k_{i+1}u^k_{i+3/2}}{J^k_{i+1}}\right|\right) + \frac{n^k_{i+1}u^k_{i+3/2}}{J^k_{i+1}} + \frac{(n^k_{i+1})^2}{J^k_{i+1}}\frac{m_{\rm d}D\Delta x}{2\varrho_{\rm f}}$$

and

$$\ln\left(\left|1 - \frac{n^k_i u^{k,+}_{i-1/2}}{J^k_i}\right|\right) + \frac{n^k_i u^{k,+}_{i-1/2}}{J^k_i} = \ln\left(\left|1 - \frac{n^k_i u^k_{i-1/2}}{J^k_i}\right|\right) + \frac{n^k_i u^k_{i-1/2}}{J^k_i} - \frac{(n^k_i)^2}{J^k_i}\frac{m_{\rm d}D\Delta x}{2\varrho_{\rm f}}.$$

respectively. However, bearing in mind the properties of the solution of the ODE (4.43), the sign of $X = \frac{n^k_{i+1}u^{k,-}_{i+3/2}}{J^k_{i+1}} - 1$ (resp. $X = \frac{n^k_i u^{k,+}_{i-1/2}}{J^k_i} - 1$) should be the same as the sign of $\frac{n^k_{i+1}u^k_{i+3/2}}{J^k_{i+1}} - 1$ (resp. $\frac{n^k_i u^k_{i-1/2}}{J^k_i} - 1$) due to the uniqueness of the Cauchy problem. We are thus led to solve equations of the general form

$$Xe^X = \bar{X}e^{\bar{X}}\ e^\alpha,$$

where $\bar{X}$ represents the known quantities, namely depending on $u^k_{i-1/2}, u^k_{i+3/2}, J^k_i, n^k_i, J^k_{i+1}, n^k_{i+1}$ and $\alpha = \frac{m_{\rm d}}{\varrho_{\rm f}}D\Delta x\frac{(n^k_{i+1})^2}{J^k_{i+1}}$ or $\alpha = -\frac{m_{\rm d}}{\varrho_{\rm f}}D\Delta x\frac{(n^k_i)^2}{J^k_i}$. The equation makes sense provided the right

hand side belongs to the range of the function $X \mapsto Xe^X$: we thus require $\bar{X}e^{\bar{X}}\, e^{\alpha} \geq -1/e$. It appears as a possible restriction on the step size Δx, depending on the sign of the data $\bar{X}$ and the current J_i^k, J_{i+1}^k. The solution X is then given by the Lambert function $X = \mathscr{W}(\bar{X}e^{\bar{X}}\, e^{\alpha})$, which lies in the same domain as the data $\bar{X}$ (if $\bar{X} < -1$, we choose the branch $\mathscr{W}_{-1}$ of the Lambert function, if $\bar{X} > -1$, then we work with the standard branch $\mathscr{W}_0$.)
The modified discrete source (4.41) is indeed consistent with the actual source term. Indeed, the leading order in $\Delta x \tilde{S}_{i+1/2}^k$ reads

$$-\partial_1 \mathbf{G}(u_{i+3/2}^k, u_{i+1/2}^k)(u_{i+3/2}^{k,-} - u_{i+3/2}^k) + \partial_2 \mathbf{G}(u_{i+1/2}^k, u_{i-1/2}^k)(u_{i-1/2}^{k,+} - u_{i-1/2}^k).$$

But, from the ODE $\partial_x \Phi(u) = -m_{\mathrm{d}} D/\varrho_{\mathrm{f}}$, we infer that $\frac{m_{\mathrm{d}}}{\varrho_{\mathrm{f}}} D\Delta x$ is approximately

$$\Phi'_{i+1}(u_{i+3/2}^k)(u_{i+3/2}^{k,-} - u_{i+3/2}^k), \qquad \text{and} \qquad \Phi'_i(u_{i-1/2}^k)(u_{i-1/2}^k - u_{i-1/2}^{k,+}),$$

respectively. Therefore, $\Delta x \tilde{S}_{i+1/2}^k$ is intended to be close to

$$-\frac{m_{\mathrm{d}}}{\varrho_{\mathrm{f}}} D\Delta x \Big(\partial_1 \mathbf{G}(u_{i+3/2}^k, u_{i+1/2}^k) \frac{1}{\Phi'_{i+1}(u_{i+3/2}^k)} + \partial_2 \mathbf{G}(u_{i+1/2}^k, u_{i-1/2}^k) \frac{1}{\Phi'_i(u_{i-1/2}^k)} \Big).$$

As Δx goes to 0 this is thus consistent to

$$-\frac{m_{\mathrm{d}}}{\varrho_{\mathrm{f}}} D\Delta x \Big(\partial_1 \mathbf{G}(u,u) \frac{1}{\Phi'(u)} + \partial_2 \mathbf{G}(u,u) \frac{1}{\Phi'(u)} \Big),$$

with $\Phi'(u) = -u/(J - nu)$. However, the flux consistency $\mathbf{G}(u,u) = u^2/2$ yields $\partial_1 \mathbf{G}(u,u) + \partial_2 \mathbf{G}(u,u) = u$, which allows us to conclude that $\Delta x \tilde{S}_{i+1/2}^k$ is consistent to $\frac{m_{\mathrm{d}}}{\varrho_{\mathrm{f}}} D(J - nu)\Delta x$.

Further details can be found in [36, Section 11]. This approach looks appealing since it preserves equilibria; however it leads to several practical difficulties. Firstly, the stationary problem does not always admit admissible solutions (in which case we keep the usual definition of the fluxes: instead of calculating the source term with (4.42) we use the standard discretization detailed at the beginning of the Section[1]). Secondly, the computational cost of the evaluation of the Lambert function is by far not negligible and it seriously impacts the computational time. Finally extending this approach to systems is not direct (see [11, 21] for a simpler case of relaxation).

4.5 Vlasov–Euler system for thin sprays

We adapt the method to handle the coupling with the Euler system. We use the BBC scheme, which is based on a Lagrange/projection algorithm on staggered grids: density and pressure are stored on the grid points x_i, the velocity is stored at the interfaces $x_{i+1/2}$. Furthermore, the scheme also involves evaluation of the velocity at intermediate time steps, in the spirit of a leap-frog approach. This idea dates back to [66], and it is intensively used in industrial hydrocodes [23, 29, 45, 61]. This is the reason why we discuss the coupling within such a

[1]Note that we consider applications far from equilibrium where particles and fluid are not yet at equilibrium. Hence, it is not that surprising not to get solutions of the stationary problem for any time.

staggered framework (see also [1, 62] where different approaches are developed for particulate flows still using staggered discretizations). We refer to [23] for further consistency analysis of such schemes. In order to explain how the scheme works it is convenient to introduce the mass variable

$$m(t,x) = \int_{x_{\min}}^{x} \rho(t,y)\,\mathrm{d}y$$

and the specific volume $\tau(t,x) = 1/\rho(t,x)$. Then, the Euler system can be recast as

$$\begin{aligned} &\mathrm{D}_t\tau - \partial_m u = 0,\\ &\mathrm{D}_t u + \partial_m p = \tau\frac{m_{\mathrm{d}}}{\varrho_{\mathrm{f}}}D(J-nu), \end{aligned}$$

where $\mathrm{D}_t = \partial_t + u\partial_x$ stands for the Lagrangian derivative. The prediction-correction algorithm becomes:

- *Step 1.1: Prediction of the fluid quantities.*
  We define the discrete mass variable and its increment

$$m_i^k = \Delta x \sum_{\ell=0}^{i} \rho_\ell^k, \qquad \Delta m_i^k = \Delta x \rho_i^k.$$

  In order to improve accuracy at low cost, the velocity is first calculated on a time step $\frac{\Delta t}{4}$, with

$$u_{i+1/2}^{k+1/4} = u_{i+1/2}^k - \frac{2\Delta t}{4(\Delta m_{i+1}^k + \Delta m_i^k)}(p_{i+1}^k - p_i^k) + \frac{\Delta t}{4}g + \frac{2\Delta t\Delta x}{4(\Delta m_{i+1}^k + \Delta m_i^k)}S_{i+1/2}^k.$$

  The source term can be treated by any of the methods detailed above. In the correction part, where the hydrodynamics quantities will be evaluated on a moving grid, there are difficulties to implement the well-balanced and the mass conservation approaches. For this reason, we adopt the simple definition of the source term by the arithmetic mean (first item of the previous section).

  Having at hand the updated velocity, we define the Lagrangian grid by

$$\xi_{i+1/2}^{k+1/2} = x_{i+1/2} + \frac{\Delta t}{2}u_{i+1/2}^{k+1/4}, \qquad \xi_i^{k+1/2} = \frac{\xi_{i+1/2}^{k+1/2} + \xi_{i-1/2}^{k+1/2}}{2}.$$

  We impose a suitable CFL condition, see Section 4.3, so that the Lagrangian cells do not intersect. Furthermore, with such a condition the Lagrangian interface $\xi_{i+1/2}$ belongs either to the Eulerian cell $[x_{i-1/2}, x_{i+1/2}]$ or to $[x_{i+1/2}, x_{i+3/2}]$. Note also that the elementary volume Δx_i is deformed into $\Delta\xi_i^{k+1/2} = \Delta x_i + \frac{\Delta t}{2}(u_{i+1/2}^{k+1/4} - u_{i-1/2}^{k+1/4})$. Then, we update the density on half the time step by

$$\rho_i^{k+1/2} = \frac{\Delta x_i}{\Delta\xi_i^{k+1/2}}\ \rho_i^k = \frac{\rho_i^k}{1 + (\frac{\Delta t/2}{\Delta x_i})(u_{i+1/2}^{k+1/4} - u_{i-1/2}^{k+1/4})}.$$

  For the pressure we set $p_i^{k+1/2} = p(\rho_i^{k+1/2})$. Note that at this stage, the fluid quantities are known on the Lagrangian grid determined by the ξ_i's.

- *Step 1.2: Prediction of the particle distribution function.*

  We use the Semi-Lagrangian scheme to update the microscopic density $f_{i,j}^k$ on a time step $\frac{\Delta t}{2}$. This step only uses the velocity $u_{i+1/2}^k$. We get in particular $n_i^{k+1/2}$ and $J_i^{k+1/2}$ on the fixed grid $[x_{i-1/2}, x_{i+1/2}]$.

- *Step 2.1: Correction of the fluid quantities.*

  We update the velocity on half a time step, with a semi-implicit treatment of the source term

$$u_{i+1/2}^{k+1/2} = \frac{1}{1+(\Delta t/2)(m_{\rm d}D/\varrho_{\rm f})\frac{n_{i+1/2}^{k+1/2,L}}{\rho_{i+1/2}^{k+1/2}}} \left(u_{i+1/2}^k - \frac{\Delta t}{2}\frac{2}{\Delta m_{i+1}^k + \Delta m_i^k}(p_{i+1}^{k+1/2} - p_i^{k+1/2}) + \frac{\Delta t}{2} g + (m_{\rm d}D/\varrho_{\rm f})\frac{\Delta t}{2\rho_{i+1/2}^{k+1/2}} J_{i+1/2}^{k+1/2,L} \right). \tag{4.44}$$

  However we face the difficulty that in (4.44) the macroscopic quantities are not naturally evaluated on the Lagrangian grid. Hence we set

$$\text{if } u_{i+1/2}^{k+1/4} > 0, \text{ then } \xi_{i+1/2}^{k+1/2} \in [x_{i+1/2}, x_{i+3/2}] \text{ and } n_{i+1/2}^{k+1/2,L} = n_{i+1}^{k+1/2}, \tag{4.45}$$

$$\text{if } u_{i+1/2}^{k+1/4} < 0, \text{ then } \xi_{i+1/2}^{k+1/2} \in [x_{i-1/2}, x_{i+1/2}] \text{ and } n_{i+1/2}^{k+1/2,L} = n_i^{k+1/2}. \tag{4.46}$$

  We define similarly $J_{i+1/2}^{k+1/2,L}$. Then, we update the density on the entire time step by

$$\xi_{i+1/2}^{k+1} = x_{i+1/2} + \Delta t(u_{i+1/2}^{k+1/2} - u_{i-1/2}^{k+1/2}), \qquad \Delta\xi_i^{k+1} = \xi_{i+1/2}^{k+1} - \xi_{i-1/2}^{k+1},$$
$$\rho_i^{k+1} = \frac{\Delta x_i}{\Delta\xi_i^{k+1}}\rho_i^k = \frac{\rho_i^k}{1+(\Delta t/\Delta x_i)(u_{i+1/2}^{k+1/2} - u_{i-1/2}^{k+1/2})},$$

  and we set $p_i^{k+1} = p(\rho_i^{k+1})$. Finally the updated velocity is given by

$$u_{i+1/2}^{k+1} = 2u_{i+1/2}^{k+1/2} - u_{i+1/2}^k. \tag{4.47}$$

  Notice that during all this procedure, we work with the mass increment Δm_i^k evaluated at t^k (thanks to the mass conservation on the Lagrangian grid). We end with a projection step: the hydrodynamic quantities are projected back on the Eulerian grid. This can be performed by incorporating a second order method with limiters.

- *Step 2.2: Correction of the particle distribution function.*

  We use the "xvx" directional splitting and the Semi-Lagrangian method to update the particle distribution function $f_{i,j}^n$ on a time step Δt. We point out that the friction term should be evaluated by using the projection on the Eulerian grid of the intermediate (Lagrangian) velocity $u_{i+1/2}^{k+1/2}$.

5 Numerical results

We present here a few simulations with both the Vlasov-Burgers and the Vlasov-Euler systems.

5.1 Vlasov–Burgers system

In the following simulation, we wish to evaluate the ability of the code to deal with the particle trajectory crossing (PTC) problem. This is a classical benchmark in which, at given time and position, particles can be found with different velocities, with opposite directions. We remind that pressureless hydrodynamic models fail in capturing such effects [44, 49]. We investigate the situation presented in [49] with the following parameters, working with dimensionless variables:

- the domain is $[-0.5, 0.5]$,
- the initial particle distribution function is $n(0,x)\delta(v = V(0,x))$, with $n(0,x) = e^{-25x^2}$ and $V(0,x) = -\sin(2\pi x)|\sin(2\pi x)|$. Consequently, particles on the right (resp. left) part of the domain move with negative (resp. positive) velocities.
- The particle mass is $m_{\rm d} = 1$, and we set $\varrho_{\rm f} = 1$ for the mass density of the fluid.
- The fluid velocity corresponds to a shock traveling from left to right : $u(0,x) = \mathbf{1}_{x\geq 0}(-x)$ (see Fig. 11),
- The numerical parameters are $N_x = 400$ and $N_v = 200$.

In [49], the benchmark is addressed by using a dedicated level set method. The particle distribution function is described through a density function and a level set distribution, the zeroes of the level set define the macroscopic velocity of the disperse phase. Transport terms are treated with a high-resolution up-wind method, incorporating ENO-limiters. We point out that the method used in [49] does not guaranty mass conservation. By contrast, we shall use the discretisation of the source term based on (4.35) so that mass is exactly conserved. In terms of (formal) spatial accuracy, the method in [49] is second order (when limiters do not act), while the Semi-Lagrangian schemes we shall use are third order accurate (but the scheme for the fluid quantities is second order).

We first perform a simulation without any drag effects by taking $D = 0$. Due to the initialization, we expect the particles to cross. On Fig. 12a-12b we observe at $t = 0.1$, two peaks in the particle density $n(t,x) = \int f dv$, which correspond to the positions where the particles have the higher velocities at the initialization (around $x = \pm 0.2$). At $t = 0.5$, the particles have crossed (now, on the left part of the domain the particles have negative velocities and on the right part of the domain they have positives velocities). Since $D = 0$ the particles have no action on the fluid motion; the shock is simply transported. The two Semi-Lagrangian methods give similar results on this test. As expected, PPM2 is slightly less diffusive than PFC3, but oscillations appear on the particle density profile. As said elsewhere this is due to the strong gradients of the initial data (here Dirac masses), which make a more diffusive method, like PFC3-NO, more adapted to the test.

Next, we perform several simulations where we make the drag coefficient D vary ($S_t = 1/D$ in [49]): $D = 10$ (high drag), $D = 1$ and $D = 0.1$ (low drag) ; the larger D, the stronger the coupling. Results are reported in Fig. 13 ($D = 10$), Fig. 14 ($D = 1$) and Fig. 15 ($D = 0.1$). We compare the density and velocity profiles by the PPM2 and PFC3 methods

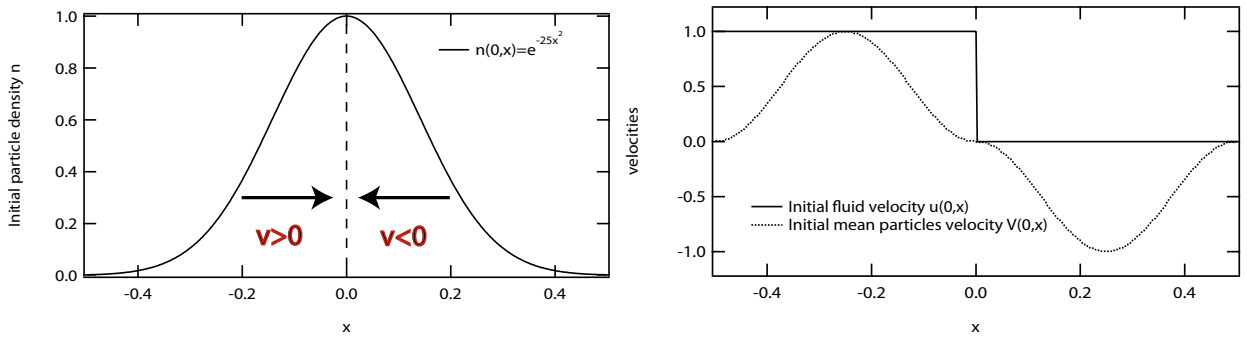

Figure 11: Initial conditions for the PTC test: particles density (left) and velocity profiles (right).

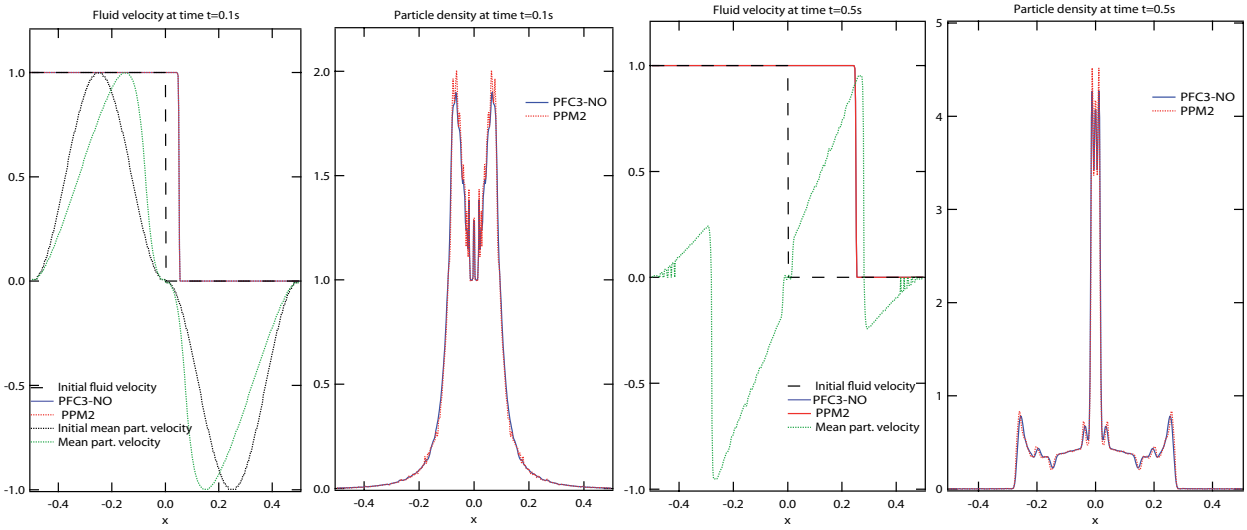

(a) Results at time $t = 0.1$ s. (b) Results at time $t = 0.5$ s.

Figure 12: Dragless simulation: Particle density (right) and velocity profiles (left) at different time.

to the results obtained in [49]. Results are in good agreement for both the macroscopic quantities and the fluid velocity. Discrepancies appear for strong drag ($D = 10$) at $t = 0.5$: Liu's density profile is more diffuse, while the evolution of the position of the particles remains similar. PFC3 and PPM2 provide quite similar results, but PPM2 produces some oscillations in density profiles. Again, this is due to the fact that PPM2 diffuses less regions of strong gradients and the initial state has Dirac masses in velocity. Compared to results in [49], the maximal particle density is slightly lower, while we remind that the total particle mass is conserved contrarily to Liu's simulations. We clearly observe different behaviors as D varies: the smaller D, the closer the behavior to the drag-free case. When reducing D, particle velocity and fluid velocity do not equilibrate on the simulation time scale and the PTC phenomena is significantly sensible, see Fig. 14 and Fig. 15. On the contrary, when $D = 10$, Fig. 13, fluid and particle velocities are at equilibrium at the end of the simulation, particles are quickly carried away by the fluid, without having time to cross. These comments can

be strengthened by looking at Fig. 16 which compares the macroscopic quantities for $D = 1$ and $D = 10$. If we focus now on the fluid velocity, with $D = 0.1$, the shock propagates, scarcely modified by the particles flow; with $D = 1$, we begin to see the interaction effects: the shock propagation is perturbed due to the drag source term, and finally with $D = 10$ the shock is strongly affected by the particles at the middle of the domain.

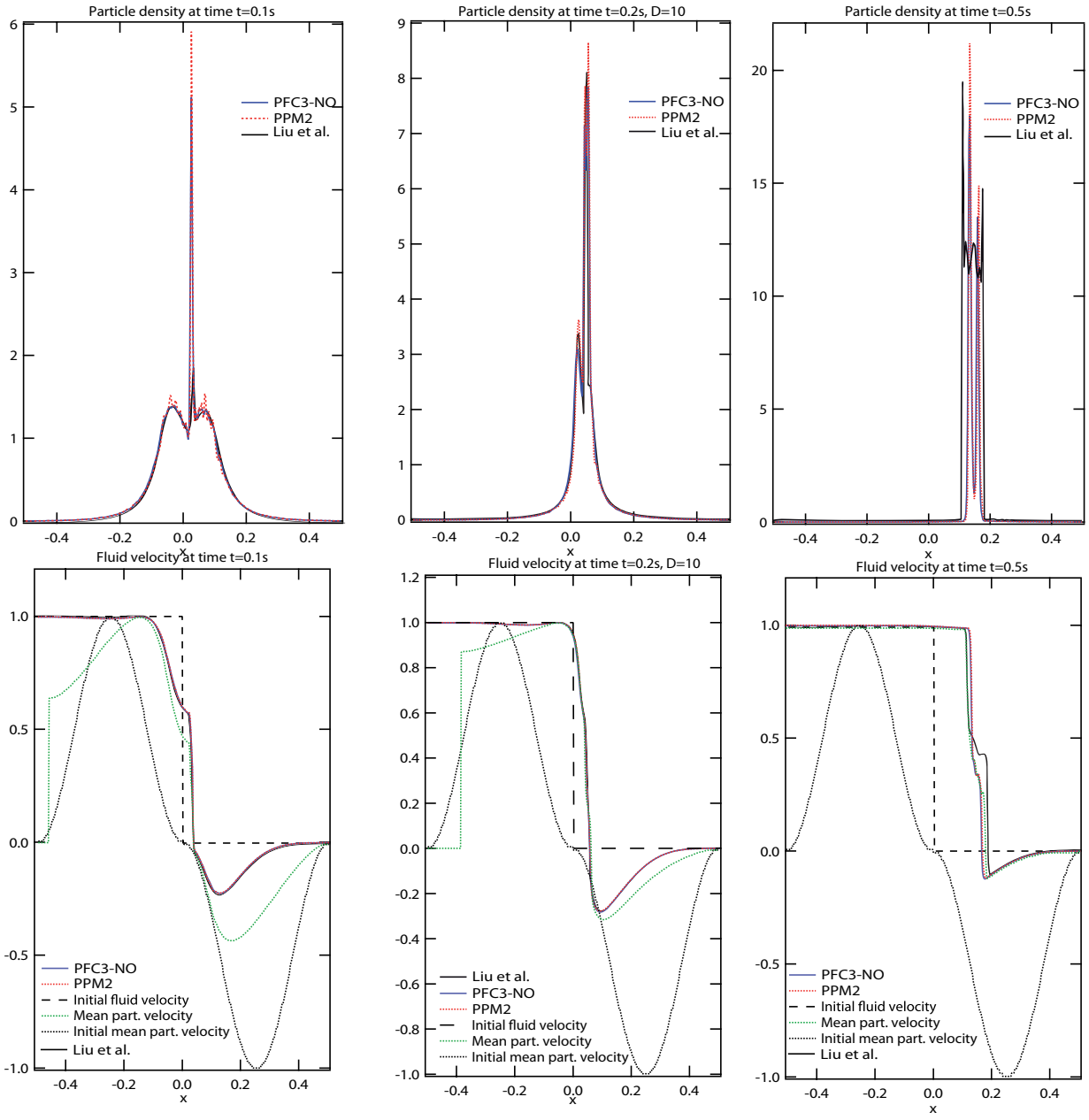

Figure 13: Vlasov-Burgers system with drag coefficient $D = 10$. Results at time $t = 0.1$ (left), $t = 0.2$ (middle) and $t = 0.5$ (right). Comparison between PPM2, PFC3 and results from [49].

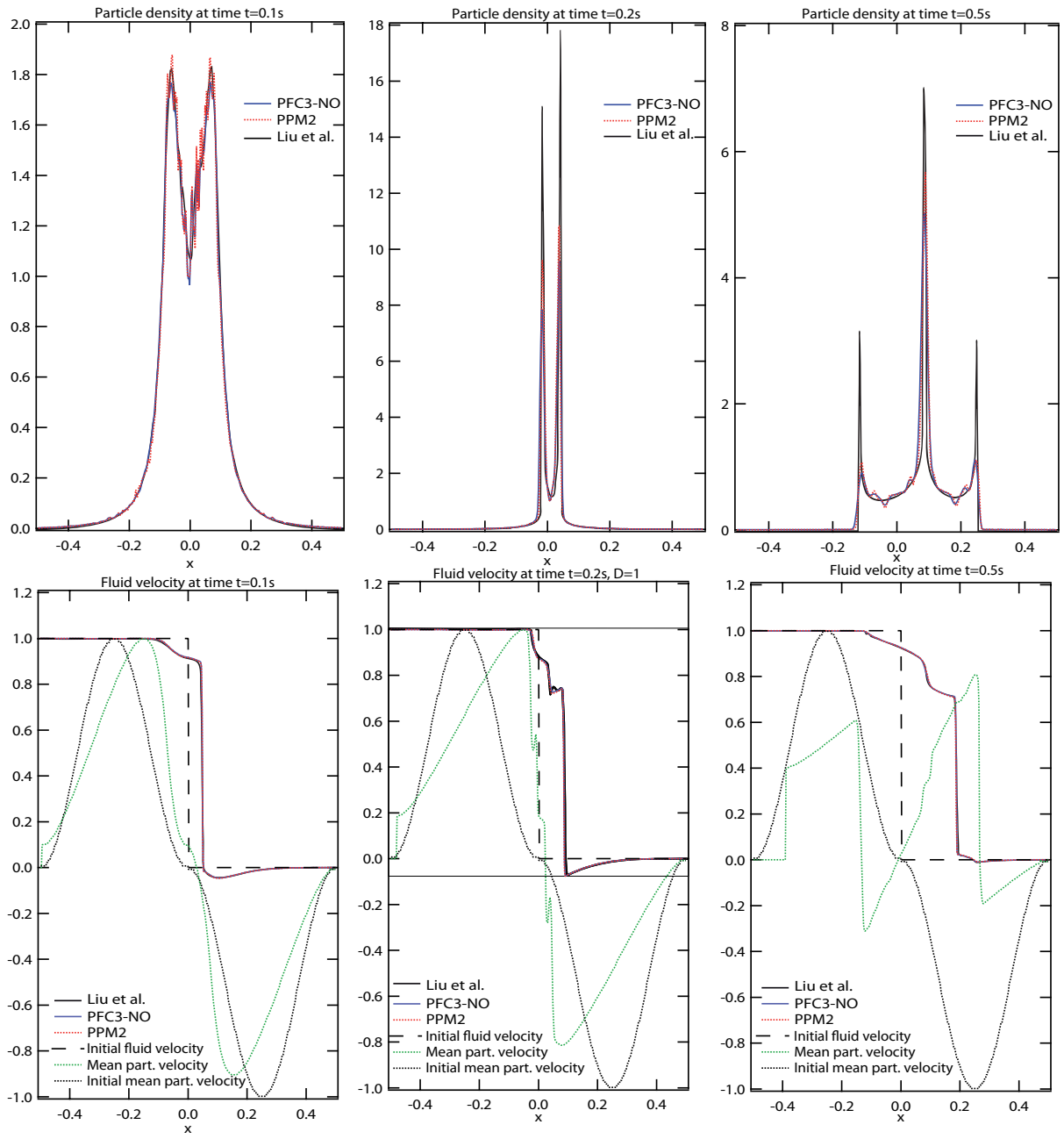

Figure 14: Vlasov-Burgers system with drag coefficient $D = 1$. Results at time $t = 0.1$ (left), $t = 0.2$ (middle) and $t = 0.5$ (right). Comparison between PPM2, PFC3 and results from [49].

Finally, we compare the results obtained with different treatments of the source terms in Fig. 17: it shows the solutions for a strong drag force $D = 10$ at the final time $t = 0.5$. Here we use the simple arithmetic mean or the method that guarantees mass conservation. We observe some discrepancies with the PFC3-NO scheme, while the results are similar

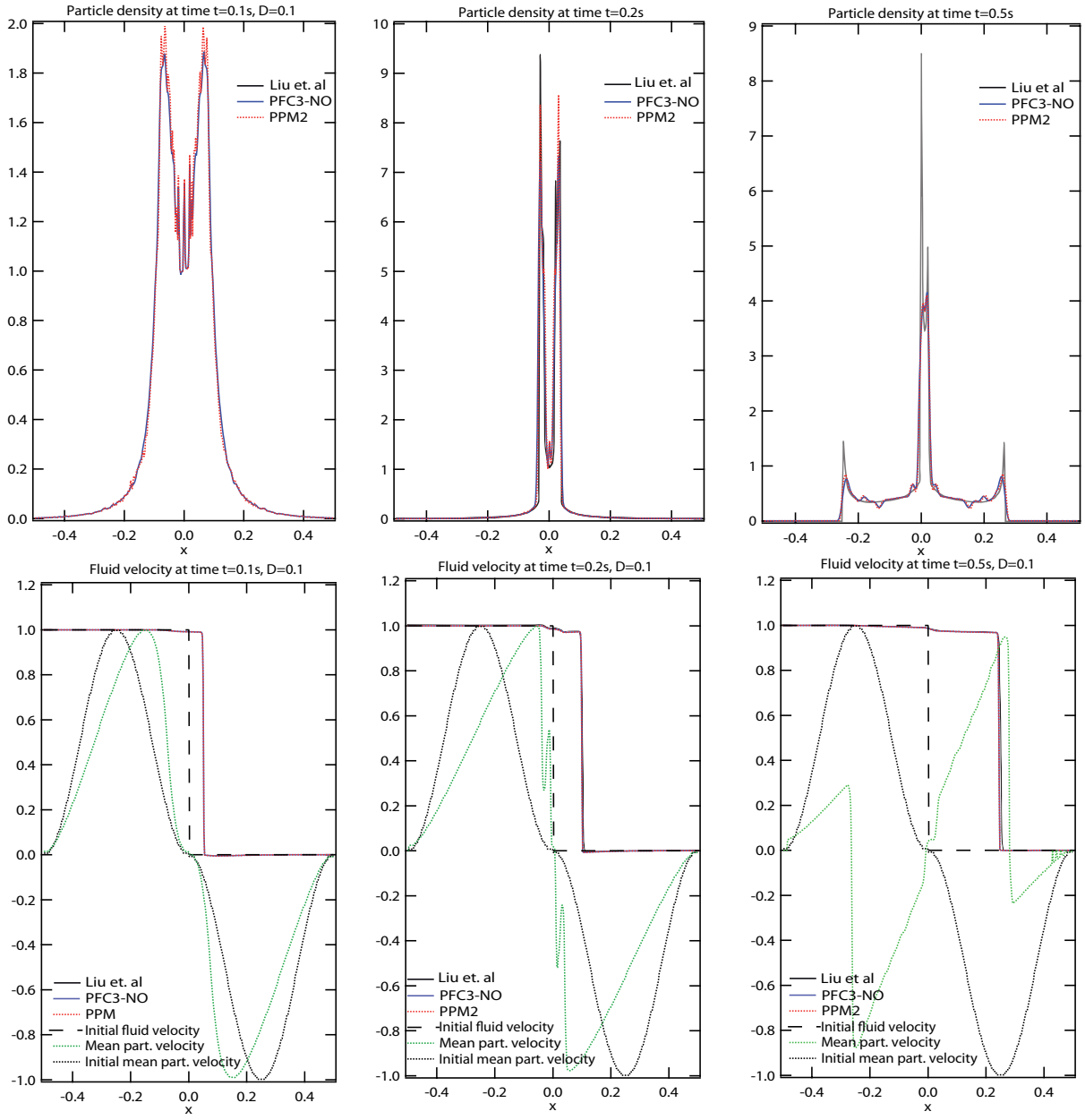

Figure 15: Vlasov-Burgers system with drag coefficient $D = 0.1$. Results at time $t = 0.1$ (left), $t = 0.2$ (middle) and $t = 0.5$ (right). Comparison between PPM2, PFC3 and results from [49].

with PPM2.

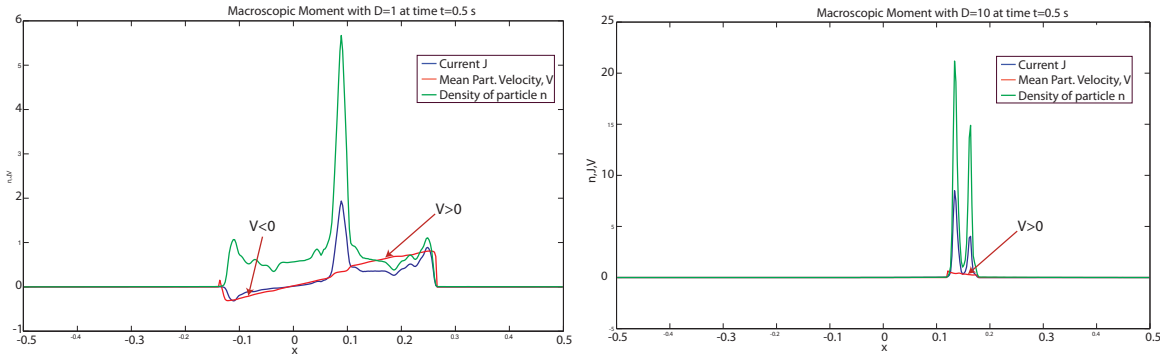

(a) $D = 1$ (b) $D = 10$.

Figure 16: Vlasov-Burgers system, mean density of particle $\int f dv$, particle current $J = \int f v dv$ and mean particle velocity with the PPM2 method at time $t = 0.5$: $D = 1$ (left), and $D = 10$ (right).

5.2 Vlasov–Euler system for thin sprays

This section considers the more realistic model involving the isentropic Euler system (2.9) for describing the fluid flow. We work with the perfect gas law for the pressure $p(\rho) = \rho^\gamma$, with $\gamma = 1.4$. The simulation domain is the slab $[0, 2]$ (but some figures restrict to the region $[0.5, 1.5]$). We deal with a shock tube with Mach number $M = 1.3$; the Riemann data are:

$$(\rho_L, u_L, p_L) = (0.54, 1.54, 1.54^\gamma) \text{ for } x < 1 \text{ and } (\rho_R, u_R, p_R) = (0, 1, 1) \text{ for } x > 1.$$

Right after the shock front, there is a layer of particles at rest: the width of the layer is 0.02, see Fig. 18, and we set $\varrho_{\rm d} = 1050$ and $r_d = 10^{-3}$. It leads to set $D = 0.6$. Accordingly the strength of the drag force exerted on the particles is strong: $\frac{D}{m_d} \sim 10^5$. The test case models the interaction of a particle cloud with a shock wave, a typical situation of interest for the applications. The numerical parameters are $N_x = 400$ and $N_v = 151$ and we present results obtained with the PPM2 and the PFC3-NO methods.

Results are displayed in Fig. 19 to 22. On the one hand, particles are put in motion when the shock crosses the cloud. On the other hand, the presence of particles induces an increase of the fluid density behind the cloud at short times. We observe that the shock is strongly affected by the particles. A reflected shock is going back from the cloud that behaves like a "porous wall", progressively put in motion, whereas a transmitted shock progresses towards the right end of the domain, see Fig. 21. Indeed, due to the drag effects, the mean particle velocity (initially equal to 0) progressively equilibrates with the velocity of the gas. Thus, at $t = 1.101$, the value of the mean particle velocity is at equilibrium with the gas velocity at the same time, see Fig. 22. Additionally, since particles on the left side of the cloud are put in motion first, we can observe an increase of the particle density. After the crossing of the shock, the cloud is simply transported. Concerning numerical comments, results with PFC3-NO or PPM2 are very similar. Nevertheless the PFC3-NO method is more diffusive; in particular it produces smaller maximal values for the particle density with a cloud more spread.

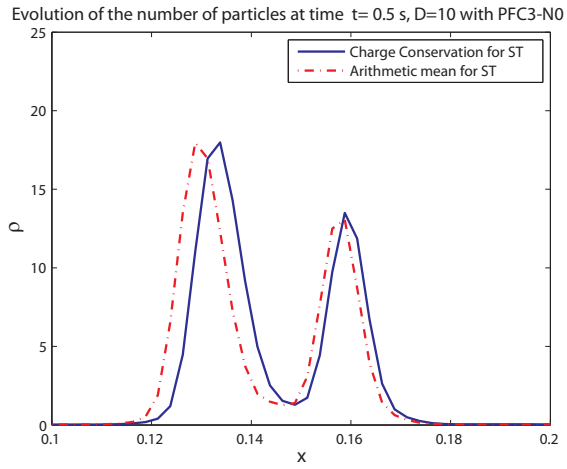

(a) Density with PFC3-NO

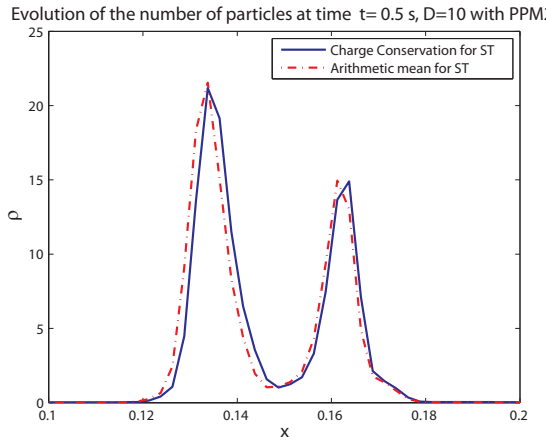

(b) Density with PPM2

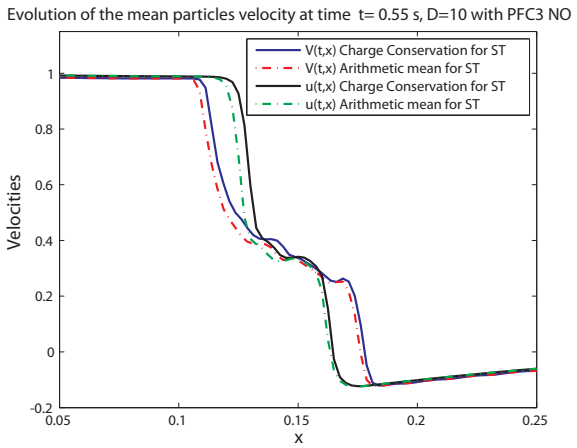

(c) Velocities with PFC3-NO

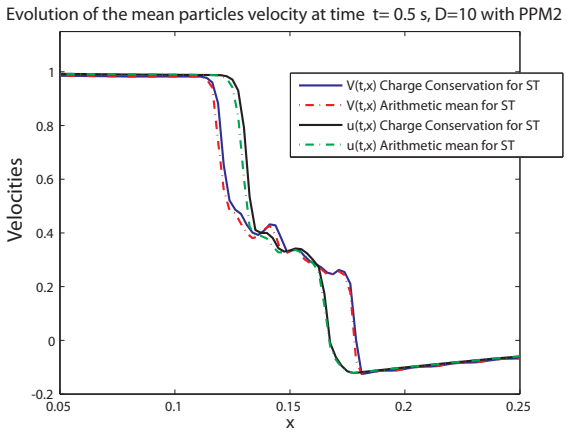

(d) Velocities with PPM2

Figure 17: Vlasov-Burgers system, comparison for $D = 10$ at $t = 0.5$ of the solutions obtained with different treatment of the source term.

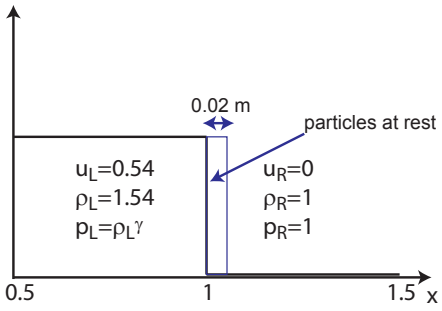

Figure 18: Initialization of the shock tube.

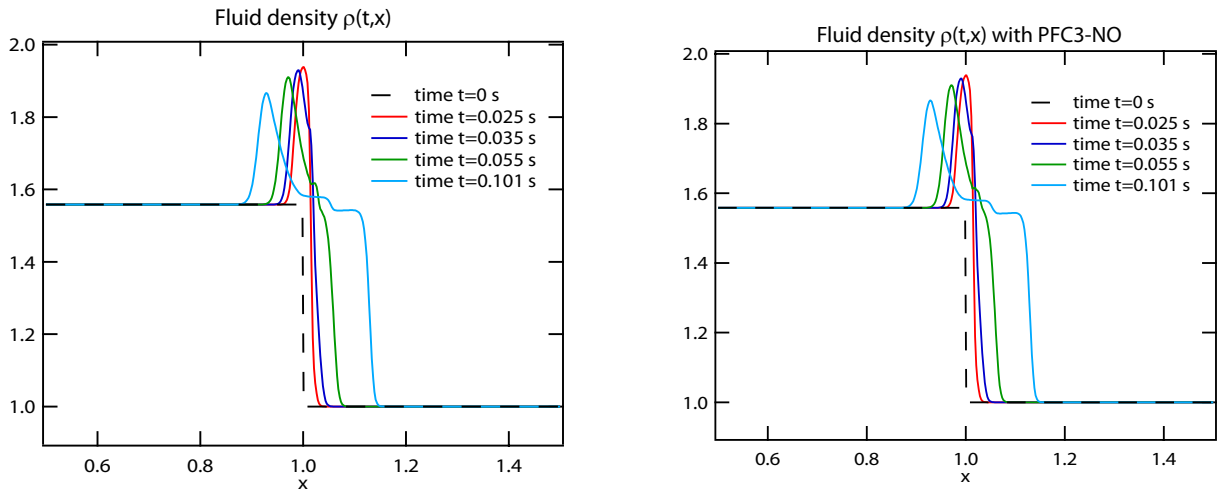

Figure 19: Vlasov-Euler system: Fluid density at different times with PPM2 (left) and PFC3-NO (right).

6 Conclusion

We have designed a scheme to solve coupled fluid-kinetic systems describing the dynamics of thin sprays. The approximation of the Vlasov-like equation for the particle distribution function is based on Semi-Lagrangian techniques, with the difficulty that phase space volumes are not conserved. The fluid equations are treated by methods working on staggered grids, as it is common in industrial hydrocodes, and we discuss how to handle the numerical coupling within this framework. The method is evaluated on several relevant benchmarks, showing the ability of the scheme in treating Particle Cross Trajectories effects, shock waves interaction with particle clouds and a wide range of drag coefficients. Extension to more intricate models, including the modelling of thick sprays, will be addressed elsewhere [6].

References

[1] M. J. Andrews and P. J. O'Rourke. The multiphase particle-in-cell (MP-PIC) method for dense particulate flows. *InJ. Multiphase Flow*, 22(2):379–402, 1996.

[2] T. D. Arber and R. G. L. Vann. A critical comparison of Eulerian-grid-based Vlasov solvers. *J. Comput. Phys.*, 180(1):339–357, 2002.

[3] C. Baranger, G. Baudin, L. Boudin, B. Després, F. Lagoutière, F. Lapébie, and T. Takahashi. Liquid jet generation and break-up. In S. Cordier, T. Goudon, M. Gutnic, and E. Sonnendrücker, editors, *Numerical Methods for Hyperbolic and Kinetic Equations*, volume 7 of *IRMA Lectures in Mathematics and Theoretical Physics*. EMS Publ. House, 2005.

[4] C. Baranger, L. Boudin, P.-E. Jabin, and S. Mancini. A modeling of biospray for the upper airways. *ESAIM:Proc*, 14:41–47, 2005.

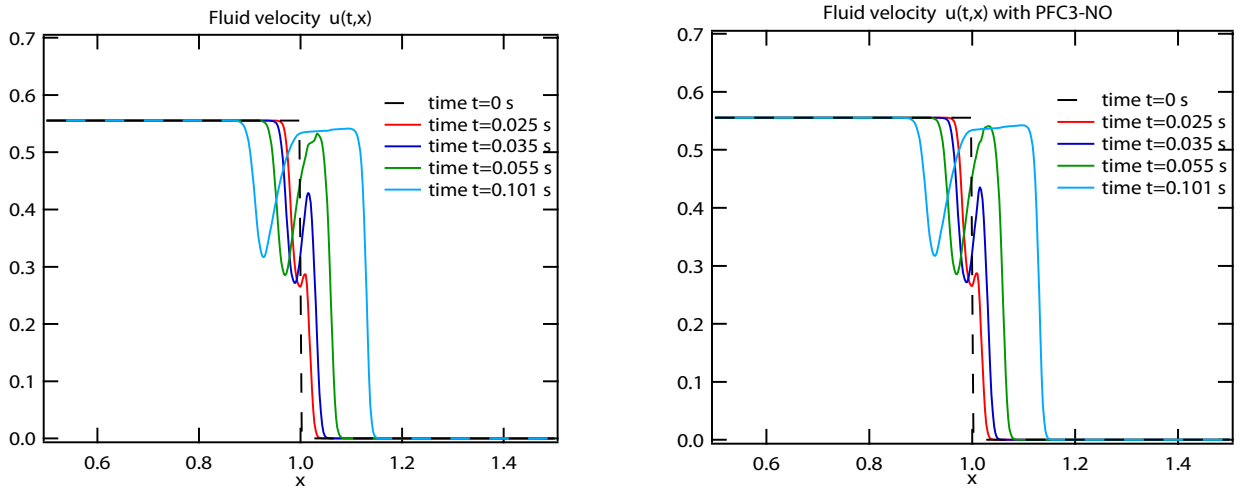

Figure 20: Vlasov-Euler system: fluid velocity at different times with PPM2 (left) and PFC3-NO (right).

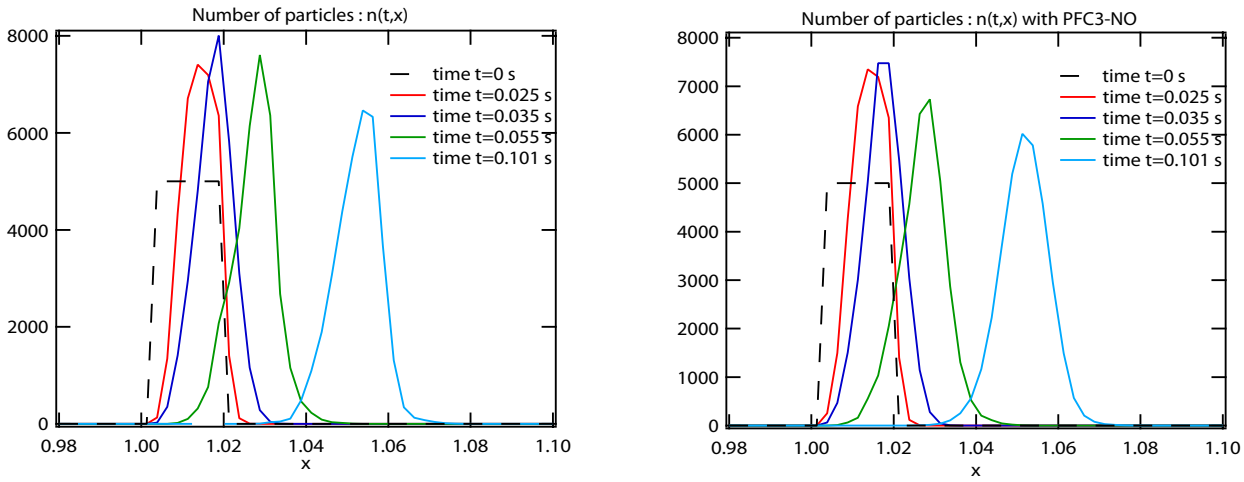

Figure 21: Vlasov-Euler system: particle density at different times with PPM2 (left) and PFC3-NO (right).

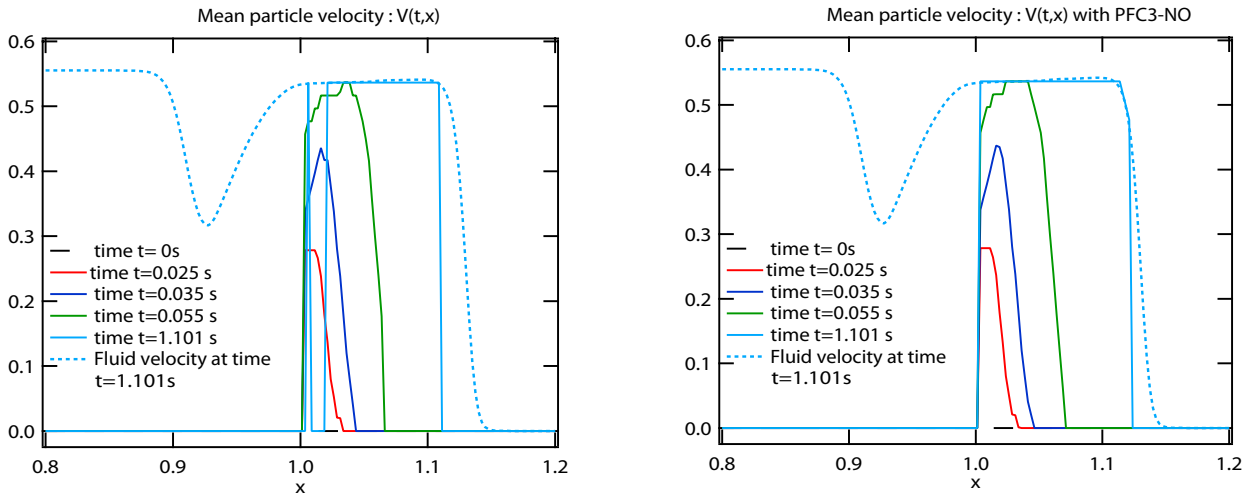

Figure 22: Vlasov-Euler system: particle velocity at different times with PPM2 (left) and PFC3-NO (right).

[5] C. Baranger and L Desvillettes. Coupling Euler and Vlasov equations in the context of sprays: local smooth solutions. *Journal of Hyperbolic Differential Equations*, 3(1):1–26, 2006.

[6] A. Bernard-Champmartin, J.-P. Braeunig, C. Fochesato, and T. Goudon. A semi-Lagrangian method for the simulation of thick sprays. Work in preparation.

[7] S. Berres, R. Bürger, and E. M. Tory. Mathematical model and numerical simulation of the liquid fluidization of polydisperse solid particle mixtures. *Comput. Visual Sci.*, 6:67–74, 2004.

[8] F. Berthelin, T. Goudon, and S. Minjeaud. Multifluid flows: a kinetic approach. Technical report, Univ. Nice Sophia Antipolis, CNRS, Inria, 2013. Work in preparation.

[9] N. Besse and E. Sonnendrücker. Semi-Lagrangian schemes for the Vlasov equation on an unstructured mesh of phase space. *J. Comput. Phys.*, 191(2):341–376, 2003.

[10] R. Botchorishvili, B. Perthame, and A. Vasseur. Equilibrium schemes for scalar conservation laws with stiff sources. *Math. Comp.*, 72:131–157, 2003.

[11] F. Bouchut, H. Ounaissa, and B. Perthame. Upwinding of the source term at interfaces for Euler equations with high friction. *Computers and Math. with Appl.*, 53:361–375, 2007.

[12] L. Boudin, B. Boutin, B. Fornet, T. Goudon, P. Lafitte, F. Lagoutière, and B. Merlet. Fluid-particles flows: A thin spray model with energy exchanges. *ESAIM: Proc.*, 28:195–210, 2009.

[13] L. Boudin, L. Desvillettes, C. Grandmont, and A. Moussa. Global existence of solutions for the coupled Vlasov and Navier-Stokes equations. *Differential and Integral Equations*, 22(11–12), 2009.

[14] J.-P. Braeunig, N. Crouseilles, V. Grandgirard, G. Latu, M. Mehrenberger, and E. Sonnendrücker. Some numerical aspects of the conservative PSM scheme in a 4D drift-kinetic code. Technical report, Inria, 2009. Report Inria RR 7109, available on `ArXiV:1303.2238`.

[15] Y. Brenier and E. Grenier. Sticky particles and scalar conservation laws. *SIAM J. Numer. Anal.*, 35(6):2317–2328 (electronic), 1998.

[16] C. Calgaro, E. Creusé, and T. Goudon. Simulation of mixture flows : Application to avalanches. Technical report, Inria, 2012.

[17] R. L. Carpenter, K. K. Droegemeier, P. R. Woodward, and C. E. Hane. Application of the piecewise parabolic method (PPM) to meteorological modeling. *Mon. Wea. Rev.*, 118(3):586–612, 1990.

[18] J. A. Carrillo and T. Goudon. Stability and asymptotic analysis of a fluid-particle interaction model. *Comm. PDE.*, 31(9):1349–1379, 2006.

[19] J.-A. Carrillo, T. Goudon, and P. Lafitte. Simulation of fluid and particles flows: asymptotic preserving schemes for bubbling and flowing regimes. *J. Comput. Phys.*, 227(16):7929–7951, 2008.

[20] J. A. Carrillo and F. Vecil. Nonoscillatory interpolation methods applied to Vlasov-based models. *SIAM J. Sci. Comput.*, 29(3):1179–1206, 2007.

[21] C. Chalons, F. Coquel, E. Godlewski, P.-A. Raviart, and N. Seguin. Godunov-type schemes for hyperbolic systems with parameter-dependent source. The case of Euler system with friction. *Math. Models Methods Appl. Sci.*, 20(11):2109–2166, 2010.

[22] C. Chalons, M. Girardin, and S. Kokh. Large time step and asymptotic preserving numerical schemes for the gas dynamics equations with source terms. *SIAM J. Sci. Comput.*, 35(6):A2874–A2902, 2013.

[23] A. Champmartin-Bernard. *Modélisation et étude numérique d'écoulements diphasiques.* PhD thesis, ENS Cachan, 2011.

[24] P. Colella and M. D. Sekora. A limiter for PPM that preserves accuracy at smooth extrema. *J. Comput. Phys.*, 227:7069–7076, 2008.

[25] P. Colella and P. R. Woodward. The piecewise parabolic method (PPM) for gas-dynamical simulations. *J. Comput. Phys.*, 54(1):174–201, 1984.

[26] N. Crouseilles, G. Latu, and E. Sonnendrücker. Hermite spline interpolation on patches for a parallel solving of the Vlasov-Poisson equation. Rapport de recherche RR-5926, INRIA, 2006.

[27] N. Crouseilles, M. Mehrenberger, and E. Sonnendrücker. Conservative semi-Lagrangian schemes for Vlasov equations. *J. Comput. Phys.*, 229:1927–1953, 2010.

[28] M. De Luca. *Contribution à la modélisation de la pulvérisation d'un liquide phytosanitaire en vue de réduire les pollutions.* PhD thesis, Univ. Aix–Marseille 2, 2007.

[29] F. De Vuyst, C. Fochesato, R. Loubère, P. Rouzier, L. Saas, R. Motte, and J.-M. Ghidaglia. Staggered lagrange-remap schemes in conservative form. Technical report, LRC MESO, CEA, CMLA, ENS Cachan, 2012.

[30] L. Desvillettes. Some new results of existence for the theory of sprays. http://www.newton.ac.uk/programmes/KIT/seminars/090710001.html, 2010. Workshop "Fluid-Kinetic Modelling in Biology, Physics and Engineering", Isaac Newton Institute for Mathematical Sciences, Programme on PDEs in Kinetic Theories.

[31] B. Engquist and S. Osher. Stable and entropy satisfying approximations for transonic flow calculations. *Mathematics of Computation*, 34(149):45–75, 1980.

[32] F. Filbet and G. Russo. High order numerical methods for the space non-homogeneous Boltzmann equation. *J. Comput. Phys.*, 186(2):457–480, 2003.

[33] F. Filbet and E. Sonnendrücker. Comparison of Eulerian Vlasov solvers. *Computer Physics Communications*, 150(3):247–266, 2003.

[34] F. Filbet and E. Sonnendrücker. Numerical methods for the Vlasov equation. In F. Brezzi, A. Buffa, S. Corsaro, and A. Murli, editors, *Numerical Mathematics and Advanced Applications*, pages 459–468. Springer Milan, 2003.

[35] F. Filbet, E. Sonnendrücker, and P. Bertrand. Conservative numerical schemes for the Vlasov equation. *J. Comput. Phys.*, 172:166–187, 2001.

[36] L. Gosse. *Computing Qualitatively Correct Approximations of Balance Laws : Exponential-fit, Well-balanced and Asymptotic-preserving*. Springer, London, 2013.

[37] L. Gosse and A.-Y. Le Roux. A well balanced scheme designed for inhomogeneous scalar conservation laws. *C. R. Acad. Sci. Paris Ser. I Math.*, 323(5):543–546, 1996.

[38] T. Goudon, P.-E. Jabin, and A. Vasseur. Hydrodynamic limit for the Vlasov-Navier-Stokes equations. I. Light particles regime. *Indiana Univ. Math. J.*, 53(6):1495–1515, 2004.

[39] T. Goudon, P.-E. Jabin, and A. Vasseur. Hydrodynamic limit for the Vlasov-Navier-Stokes equations. II. Fine particles regime. *Indiana Univ. Math. J.*, 53(6):1517–1536, 2004.

[40] T. Goudon, S. Jin, and B. Yan. Simulation of fluid-particles flows: heavy particles, flowing regime, and asymptotic-preserving schemes. *Commun. Math. Sci.*, 10(1):355–385, 2012.

[41] T. Goudon, A. Moussa, L. He, and P. Zhang. The Navier–Stokes–Vlasov–Fokker–Planck system near equilibrium. *SIAM J. Math. Anal.*, 42(5):2177–2202, 2010.

[42] T. Goudon and F. Poupaud. On the modeling of the transport of particles in turbulent flows. *M2AN Math. Model. Numer. Anal.*, 38(4):673–690, 2004.

[43] J. Guterl, J.-P. Braeunig, N. Crouseilles, V. Grandgirard, G. Latu, M. Mehrenberger, and E. Sonnendrücker. Test of some numerical limiters for the conservative PSM scheme for 4D Drift-Kinetic simulations. Rapport de recherche RR-7467, INRIA, 2010.

[44] S. Hank, R. Saurel, and O. Le Metayer. A hyperbolic Eulerian model for dilute two-phase suspensions. *J. Modern Physics*, 2:997–1011, 2011.

[45] O. Heuzé, S. Jaouen, and H. Jourdren. Dissipative issue of high-order shock capturing schemes with non-convex equations of state. *J. Comput. Phys.*, 228(3):833–860, 2009.

[46] P.-E. Jabin. Large time concentrations for solutions to kinetic equations with energy dissipation. *Comm. Partial Differential Equations*, 25(3-4):541–557, 2000.

[47] G. Lavergne. *Modélisation de l'écoulement multiphasique dans le propulseur à poudre P230 d'Ariane 5*, 2004. Lecture Notes of the School of the Groupement Français de Combustion, Ile d'Oléron.

[48] J. Lighthill. Ocean spray and the thermodynamics of tropical cyclones. *J. of Engineering Math.*, 35:11–42, 1999.

[49] H. Liu, Z. Wang, and R. O. Fox. A level set approach for dilute non-collisional fluid-particle flows. *J. Comput. Phys.*, 230(4):920–936, 2011.

[50] C. K. K. Lun and S. B. Savage. *Kinetic Theory for Inertia Flows of Dilute Turbulent Gas-Solids Mixtures*, volume 624 of *Lect. Notes Phys.*, pages 267–289. Springer, 2003.

[51] J. Mathiaud. *Etude de systèmes de type gaz–particules.* PhD thesis, ENS Cachan, 2006.

[52] A. Moussa. *Etude mathématique et numérique du transport d'aérosols dans le poumon humain.* PhD thesis, ENS Cachan, 2009.

[53] P. J. O'Rourke. *Collective drop effects on vaporizing liquid sprays.* PhD thesis, Princeton University, NJ, 1981. Available as Technical Report #87545 Los Alamos National Laboratory.

[54] N. A. Patankar and D. D. Joseph. Lagrangian numerical simulation of particulate flows. *Int. J. Multiphase Flow*, 27:1685–1706, 2001.

[55] N. A. Patankar and D. D. Joseph. Modeling and numerical simulation of particulate flows by the Eulerian–Lagrangian approach. *Int. J. Multiphase Flow*, 27:1659–1684, 2001.

[56] K. Schäfer *et al.* Influences of the 2010 Eyjafjallajökull volcanic plume on air quality in the northern alpine region. *Atmos. Chem. Phys. Discuss.*, pages 9083–9132, 2011.

[57] N.J. Sircombe and T.D. Arber. Valis: A split-conservative scheme for the relativistic 2d Vlasov-maxwell system. *J. Comput. Phys.*, 228(13):4773–4788, 2009.

[58] D. M. Snider, P. J. O'Rourke, and M. J. Andrews. Sediment flow in inclined vessels calculated using a multiphase particle-in-cell model for dense particle flows. *Int. J. Multiphase Flow*, 24:1359–1382, 1998.

[59] E. Sonnendrücker, J. J. Barnard, A. Friedman, D. P. Grote, and S. M. Lund. Simulation of heavy ion beams with a semi-Lagrangian Vlasov solver. *Nuclear Instruments and Methods in Physics Research Section A: Accelerators, Spectrometers, Detectors and Associated Equipment*, 464(1–3):470–476, 2001. Proc. of the 13th Int. Symp. on Heavy Ion Inertial Fusion.

[60] E. Sonnendrücker, J. Roche, P. Bertrand, and A. Ghizzo. The semi-Lagrangian method for the numerical resolution of the Vlasov equation. *J. Comput. Phys.*, 149:201–220, 1999.

[61] W. G. Sutcliffe. BBC hydrodynamics. Technical report, California Univ., Livermore Lawrence Livermore Lab., 1974.

[62] D. J. Torres and M. F. Trujillo. KIVA-4: An unstructured ALE code for compressible gas flow with sprays. *J. Comput. Phys.*, 219:943–975, 2006.

[63] T. Umeda. A conservative and non-oscillatory scheme for Vlasov code simulations. *Earth Planets Space*, 60:773–779, 2008.

[64] T. Umeda, M. Ashour-Abdalla, and D. Schriver. Comparison of numerical interpolation schemes for one-dimensional electrostatic Vlasov code. *Journal of Plasma Physics*, 72:1057–1060, 2006.

[65] I. Vinkovic. *Dispersion et mélange turbulents de particules solides et de gouttelettes par une simulation des grandes échelles et une modélisation stochastique lagrangienne. Application à la pollution de l'atmosphère.* PhD thesis, Ecole Centrale de Lyon, 2005.

[66] J. Von Neumann and R.D. Richtmyer. A method for the numerical calculation of hydrodynamic shocks. *J. Appl. Phys.*, 21:232–237, 1950.

[67] F. A. Williams. *Combustion Theory.* Benjamin/Cummings, 1985. 2nd. edition.

[68] P. Woodward and P. Colella. The numerical simulation of two-dimensional fluid flow with strong shocks. *J. Comput. Phys.*, 54(1):115–173, 1984.